

AGGREGATION-INDUCED EMISSION IN ORGANIC NANOPARTICLES: PROPERTIES AND APPLICATIONS: A REVIEW

V. M. Granchak,¹ T. V. Sakhno,² I. V. Korotkova,³
Yu. E. Sakhno,² and S. Ya. Kuchmy¹

UDC 535.37+544.522.123

Data on the aggregation-induced emission (AIE) of organic nanoparticles are summarized. The mechanisms for the appearance of AIE in nanoparticles with a wide variety of molecular structure including hydrocarbons, compounds with heteroatoms, and organometallic complexes as well as the major factors determining the efficiency of luminescence in the solid state are examined. Applied aspects of the use of AIE are discussed.

Key words: aggregation-induced emission, aggregation-induced enhanced emission, fluorescent organic nanoparticles.

In recent decades, there has been extensive study of fluorescing inorganic semiconductors and metals, which have attracted considerable attention due to their series of unique properties arising, in particular, from quantum dimensional effects [1, 2]. Such nanoparticles may be used as fluorescent biological labels, active elements of photoelectric transducers and light emitting devices, and optical monitors [1-5].

Nano- and microcrystals of organic dyes display greater variability in their structure and physical properties than their inorganic analogs. Their chemical and photochemical stability is higher than for isolated molecules and they display unique optical and optoelectronic properties, while holding interest for various potential applications in biological probes and labels [6], photocatalysts [7], organic light emitting devices, and microresonators [8]. Unfortunately, only some of these objects emit strong fluorescence. Most organic luminophores with strong fluorescence in solution at low concentrations have much lower emission efficiency in the solid state. The formation of excimers, generation of excitons, and the migration of excitation energy to impurity sites or surface defects in solid structures sharply decrease the emission efficiency. However, there are a number of compounds, which inflammation of fluorescence in the solid state rather than quenching. Such effects were observed in a study of organosilicon compounds: penta- and tetraphenylsilols, 1-methyl-1,2,3,4,5-pentaphenylsilol [9, 10], silol-containing polyacetylenes [11], as well as other derivatives of arylethynyl [12], poly(phenyleneethynylene) [13], poly(phenylene-vinylene) [14], 1,4-bis(phenylethynyl)benzene [15], pyrazoline [16], 1-cyano-*trans*-1,2-bis(4'-methyldiphenyl)ethylene [17], 2,2'-dihydroxyazine, and barbituric acid [18-20]. The aggregation of dye molecules in solution or in the adsorbed state also may lead to a significant change in their fluorescent properties [21, 22], including the possibility of an enhanced

¹L. V. Pysarzhevsky Institute of Physical Chemistry, National Academy of Sciences of Ukraine, Nauky Ave., 31, Kyiv 03028, Ukraine. E-mail: granchakvm@ukr.net.

²Poltava University of Economics and Trade, Kovalya St., 3, Poltava 36014, Ukraine. E-mail: sakhno2001@gmail.com.

³Poltava State Agrarian Academy, Skovorody St., 1/3, Poltava 36000, Ukraine. E-mail: 2irinakorotkova10@gmail.com.

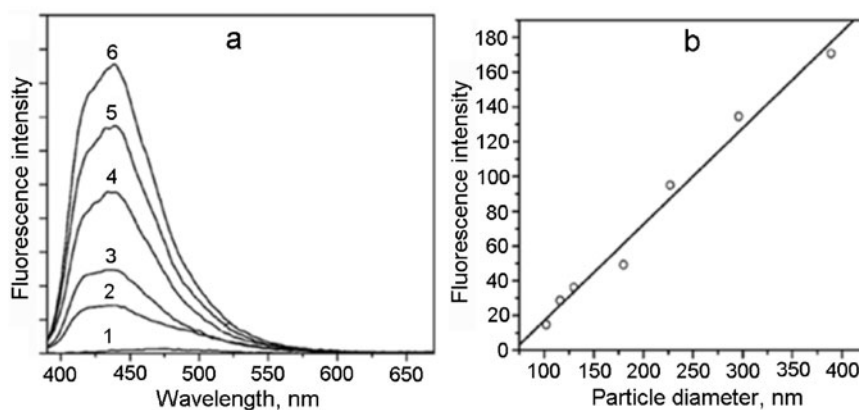


Fig. 1. a) Fluorescence spectra of nanoparticles of **2** in CHCl_3 (1) and in 1 : 1 $\text{CHCl}_3/\text{CH}_3\text{OH}$ after maintenance for 5 (2), 30 (3), 60 (4), 120 (5), and 240 min (6), b) size dependence of the fluorescence intensity of nanoparticles of **2**. Reprinted with permission [37]. Copyright © 2005, American Chemical Society.

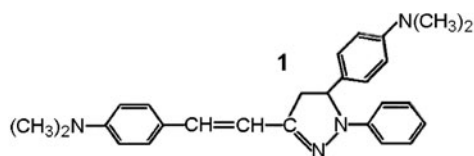
phosphorescence yield [23]. Covalently-bound dimers, namely, biscyanine dyes with conjugated chromophores, showed a previously unknown effect, namely, an enhanced fluorescence yield along with enhanced intersystem crossing [24]. Such a paradox can be attributed to a greater probability for radiative transition in comparison with nonradiative transition with increasing angle between the chromophores. The increase in the probability of population of triplet states upon the interaction of the chromophores in biscyanines has been used to obtain intense fluorescence in the near-IR spectral region due to thermoactivation of slow luminescence [25].

In the present review, we summarize the literature data on the spectral luminescence properties of aggregates and nanoparticles of organic compounds termed AIE luminogens and the possibility of application the aggregation-induced emission (AIE) effect in light emitting structures.

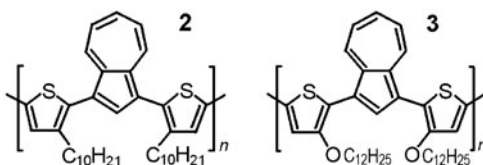
SIZE DEPENDENCE OF FLUORESCENCE PROPERTIES OF ORGANIC NANOPARTICLES

The first systematic studies of the luminescence properties of nanoparticles of perylene and phthalocyanine were carried out by Kasai et al. [26-29], who found that the fluorescence characteristics of such compounds depend significantly on the nanoparticle size. Thus, three types of bands [26, 28] identified as monomer luminescence ($\lambda_{fl} = 440$ nm), F-exciton emission ($\lambda_{fl} = 480$ nm), and S-exciton emission ($\lambda_{fl} = 560$ nm) (where F is a free exciton and S is a self-trapped exciton) are observed in the emission of perylene crystals varying in diameter from 93 to 211 nm. For crystals with diameter 50 nm, the F-exciton emission band maximum is found about 470 nm, while for particles with 200 nm diameter, the maximum is at 482 nm [27]. Furthermore, decreasing crystal size leads to an increase in the intensity of F-exciton emission relative to the intensity of S-exciton emission.

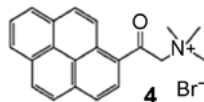
The spectral luminescence properties of 1-phenyl-3-((dimethylamino)styryl)-5-((dimethylamino)phenyl)-2-pyrazoline (**1**) also depend on the size of its nanoparticles. Thus, increasing the diameter from 20 to 310 nm leads to the appearance of a charge transfer (CT) band in the absorption spectrum, which undergoes a bathochromic shift from 438 to 455 nm [17]. A band with maximum at $\lambda_{fl} = 450$ nm is observed in a true ethanolic solution of **1** but emission bands with maximum at $\lambda_{fl} = 500$, 535, and 463 nm arise in the presence of nanoparticles of **1**, the intensity of the latter gradually decreases with increasing nanoparticle size. The redistribution of the emission intensity from the S_1 state to the state with CT with increasing nanoparticle size indicates that these states compete with each other [30-36].



Strong dependence of the absorption intensity and significant enhancement of the emission with increasing particle size were observed for monodisperse conjugated polymer nanoparticles of poly{1,3-bis[2-(3-*n*-decylthienyl)]azulene} (**2**) (Fig. 1) and poly{1,3-bis[2-(3-*n*-dodecoxythienyl)]azulene} (**3**) [37].

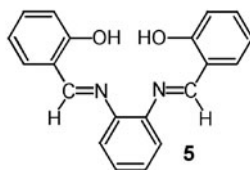


A study of nanoaggregates of trimethyl(2-oxo-2-pyren-1-ylethyl)ammonium bromide (**4**) in tetrahydrofuran (THF) in the presence of added water showed that their fluorescent properties depend not only on the dye concentration but also on the size of its nanoparticles obtained by reprecipitation, i.e., upon the addition of an aqueous solution of **4** to THF. The spectra of dilute solutions of **4** show fluorescence bands with maxima at $\lambda_{fl} = 390, 412,$ and 433 nm, which shift with increasing dye concentration toward longer wavelengths and coalesce into a single broad band with $\lambda_{fl} = 469$ nm. The observed spectral changes are related to the formation of nanoparticles of **4** and change in their size upon increasing the dye concentration. Furthermore, the position of the fluorescence bands and size of the nanoparticles of **4** formed depend also on the H₂O/THF ratio in the solvent mixture. Thus, an increase in the water content leads to a shift in the fluorescence maximum from $\lambda_{fl} = 433$ to 448 nm obtained by the addition of 0.5 mL aqueous solution of **4** to 0.5 mL THF and the appearance of a ball-shaped aggregate with diameter 450 nm [38].



A similar dependence of the fluorescent properties of **4** on its content was also observed in polyvinyl alcohol films. At low dye content (0.01 mole %), we find only emission of the monomer form ($\lambda_{fl} = 450$ nm) but the fluorescence maximum is shifted with increasing concentration to 2.0 mole % toward longer wavelengths ($\lambda_{fl} = 530$ nm), which is attributed to the emission of dimers or excimers of **4** [39, 40].

Aging of the particles, as a rule, leads to an increase in their size and greater ordering of crystal structure, which is accompanied by change in the emission properties. Thus, an increase in the fluorescence of *bis*(salicylaldehyde)-*o*-phenylenediimine (salophen) (**5**) is found upon the addition of its dioxane solution to water [36]. This behavior is related to the



formation of microtubes of salophen. In the initial step, these structures are formed with the participation of primary disordered rod-like nanoparticles with diameter 80-120 nm and length 400-600 nm, which convert over 1 h into semi-tubular structures. The formation of the microtubes is accompanied by a sharp change in the fluorescence intensity. The emission spectra of the solution of **5** in dioxane and the initial suspension of nanoparticles have two very weak bands with maxima at $\lambda_{fl} = 545$ and 435 nm. Upon aging, the intensity of the emission at $\lambda_{fl} = 545$ nm decreases and the shorter-wavelength band undergoes a bathochromic

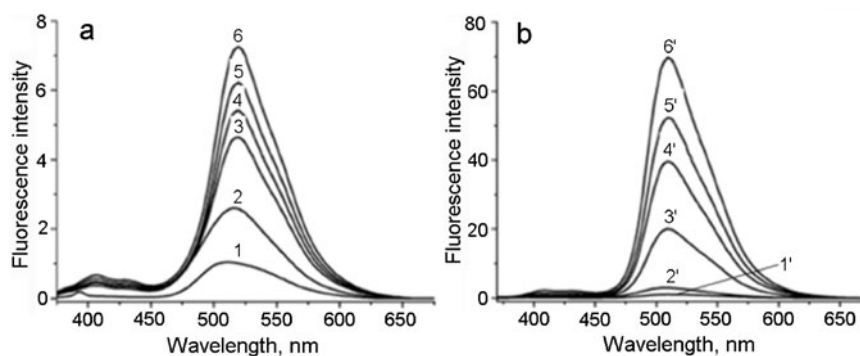
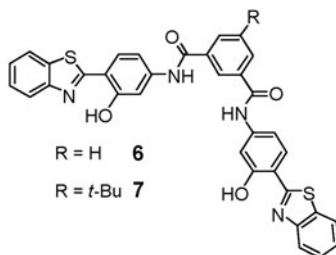


Fig. 2. Fluorescence spectra of **6** (a) and **7** (b) in tetrahydrofuran (1 and 1') and in 38 : 62 (vol.) THF/H₂O after mixing of the solutions (2 and 2') and maintenance for 1 h 40 min (3) and 26 min (3'), 4 h (4) and 55 min (4'), 9 h (5) and 1 h 30 min (5'), 21 h (6) and 6 h 20 min (6'). The scale on the y-axis is multiplied by $\times 5$ for 1 and by $\times 10$ for 1'. Reprinted with permission [42]. Copyright © 2007, American Chemical Society.

shift to 451 nm and its intensity gradually undergoes a more than 100-fold increase. The driving forces for the self-organization of these particles and their combination to give microtubes may be multiple intermolecular C–H $\cdots\pi$ interactions, which provide rigidity to the molecular structure such that “tubular” salophen becomes a stronger emitter. The mechanism of this process is similar to mechanism of “oriented binding” in the formation of nanorods of anatase (TiO₂) [41].

The differences in the emission in solutions of N,N'-di[3-hydroxy-4-(2'-benzothiazole)phenyl]isophthalic amide (**6**) and N,N'-di[3-hydroxy-4-(2'-benzothiazole)phenyl]5-*tert*-butyl-isophthalic amide (**7**) are explained by different models of molecular stacking of these compounds and the shape of the resultant aggregates, which is attributed to the presence of *tert*-butyl group and confirmed by the time-dependent recording of the fluorescence spectra of the nanoparticles/aggregates (Fig. 2) and molecular modelling [42].



The absorption spectra of dilute solutions of **6** and **7** in THF ($5 \cdot 10^{-6}$ mol/L) have a band with maxima at ~ 312 nm, which is related to excitation of the 1,3-benzothiazole fragment and another at ~ 353 nm due to electron transfer between the benzothiazole and hydroxyphenyl fragments. Two bands of unequal intensity are also observed in the emission spectra: a weak band at $\lambda_{fl} = 393$ nm is attributed to emission of the enol, while the band at $\lambda_{fl} = 509$ nm is related to the keto tautomer formed as a result of excited-state intramolecular proton transfer (ESIPT), which takes place with quantum yield 0.0021 for **6** and 0.0017 for **7** at room temperature. The addition of water to a THF solution with the same dye concentration leads to increased emission of both compounds due to changes in the shape and size of the nanoparticles. Thus, the particle diameter of **6** is about 100 nm after 2 h and 150–250 nm after 4 h, while cubic particles with specifically-ordered arrangement of molecules of **6** form after 21 h. The growth of aggregates of **7** is much more rapid: particle diameter is 20–150 nm after 15 min and 100–400 nm after 30 min, while large rectangular rods with length 280–580 nm and width ~ 80 nm are formed after 1 h.

The changes in shape and size of the nanoparticles also affect their spectral characteristics. Thus, the luminescence intensity of **7** upon aging of its solution in THF/water gradually increases with invariant position of the fluorescence maxima attributed to the keto form. After aging of the solution for 6 h, the emission quantum yield increased to 0.19, i.e., by a factor of about 112 relative to the fluorescence in pure THF ($\phi \approx 0.0017$) and by a factor of 21 relative to the initial emission intensity of **7** in THF/H₂O ($\phi \approx 0.009$). The intensity of that band with $\lambda_{fl} = 393$ nm attributed to the fluorescence of the enol also increased

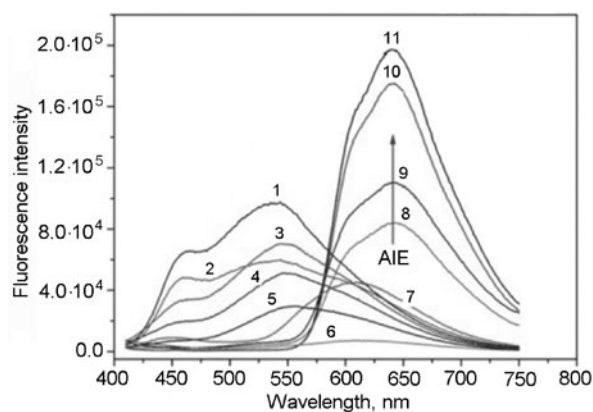
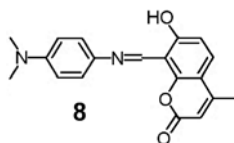


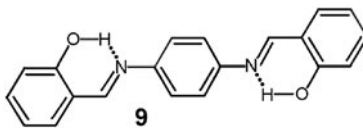
Fig. 3. Fluorescence spectra of **8** in H₂O/DMF solvent mixtures with water content 0 (1), 10 (2), 30 (3), 40 (4), 20 (5), 50 (6), 60 (7), 70 (8), 80 (9), 90 (10), and 99 vol.% (11). Reprinted with permission [43]. Copyright © 2016, The Royal Society of Chemistry.

nine-fold relative to the sample at the beginning (0 min). Aging of the solution of **6** in 38 : 62 (vol.) THF/H₂O was also accompanied by an increase in emission quantum yield from $\phi \approx 0.012$ ($\lambda_{fl} = 516$ nm) to $\phi \approx 0.029$ ($\lambda_{fl} = 519$ nm) after maintenance of the sample for 21 h [42].

As a result of the ESIPT process, fluorescent aggregates of different size are also formed in the case of 8-((4'-dimethylamino-2'-ylimino)-methyl)-7-hydroxy-4-methyl-2H-chromen-2-one (**8**), in which the proton donor (-OH) and proton acceptor groups (-C=N-) are rather close to each other. The observed red shift of the fluorescence band ($\lambda_{fl} = 604$ nm in ethanol to $\lambda_{fl} = 650$ nm in the film) is attributed to the formation of aggregates of **8**, in which rotation of the phenyl group is restricted. The formation of aggregates of molecules of **8** was observed in H₂O/DMF mixture with various water fractions. Figure 3 shows that increasing the water content to 50% leads to a decrease in the fluorescence intensity, which is related to intramolecular charge transfer in the folded conformation of the compound arising in the excited state. Enhanced emission is observed when the water content in the mixture exceeds 60% along with a shift in the emission maximum from $\lambda_{fl} = 540$ to 640 nm. The red shift and enhanced emission are attributed to formation of aggregates of **8** due to restriction of C=N isomerization and rotation of the phenyl group, which favor the ESIPT process [43].



The conversion of particles of N,N'-bis(salicylidene)-p-phenylenediamine (**9**) from nanospheres with diameter 10 nm into rod-like structures with length about 2000 nm and width 100 nm is accompanied by a more than sixty-fold enhancement of fluorescence intensity in comparison with the intensity of this compound in methanol solution [44]. We should note that the fluorescence band of **9** in CH₃OH has its maximum at $\lambda_{fl} = 535$ nm, while this band appears in water at $\lambda_{fl} = 546$ nm; its intensity depends on the aging time: the quantum yield decreases from $\phi \approx 0.06$ to $\phi \approx 0.025$ after maintenance for 6 h. The reason for this change in emission during aging of the sample is not completely clear but may be related to an interaction involving the azomethine group of one molecule with the benzene ring of another in the nanoparticle [44].



Spectral luminescent characteristics of series of other representatives of AIE luminogens are presented in Table 1.

TABLE 1. Organic Compounds Displaying AIE Luminescence

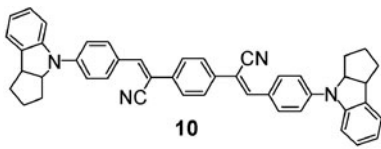
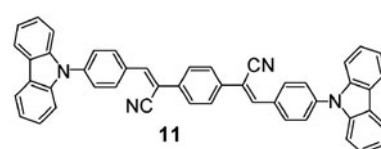
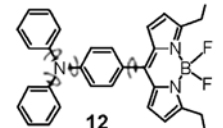
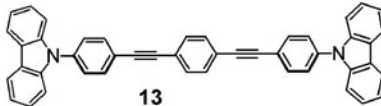
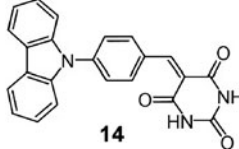
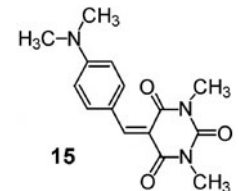
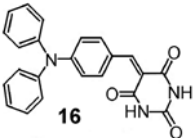
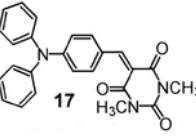
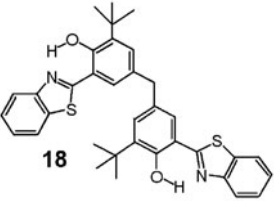
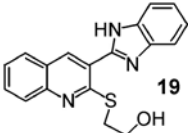
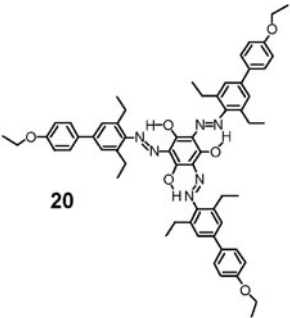
Compound	$\lambda_{\max}^{\text{abs}}$, nm (media)	$\lambda_{\max}^{\text{fl}}$, nm (media)	ϕ (media)	Ref.
 <p>10</p> <p>(2Z,2'Z)-2,2'-(1,4-Phenylene)bis(3-(4-(2,3,3a,8b-tetrahydrocyclopenta[b]indol-4(1H)-yl)phenyl)acrylonitrile)</p>	450 (THF)	545 (THF) 563 (film)	0.007 (THF) 0.51 (film)	[45]
 <p>11</p> <p>(2Z,2'Z)-2,2'-(1,4-Phenylene)bis(3-(4-(9H-carbazol-9-yl)phenyl)acrylonitrile)</p>	400 (THF)	499 (THF) 511 (film)	0.0143 (THF) 0.564 (film)	[45]
 <p>12</p> <p>(4')-Triphenylamine-1,8-diethylpyromethine-difluoroborate</p>	512 (ethanol)	653 (ethanol)	0.003 (ethanol) 0.009 (ethanol/glycerin = 1 : 9)	[46]
 <p>13</p> <p>1,4-bis(((9H-Carbazol-9-yl)phenyl)ethynyl)-benzene</p>	343 (THF)	417 (THF) 473, 593 (in solid phase)	0.06 (THF) 0.28 (powder)	[47]
 <p>14</p> <p>5-(N-Carbazolestyryl)barbituric acid</p>	412 (THF)	592 (THF) 612 (H ₂ O/THF)	0.054 (THF) 0.114 (H ₂ O/THF)	[48]
 <p>15</p> <p>5-(4-Dimethylaminostyrene)-1,3-dimethylbarbituric acid</p>	454 (THF)	542.8 (THF) 603.4 (H ₂ O/THF)	0.004 (THF) 0.082 (H ₂ O/THF)	[48]

TABLE 1. (Continued)

Compound	$\lambda_{\max}^{\text{abs}}$, nm (media)	$\lambda_{\max}^{\text{fl}}$, nm (media)	ϕ (media)	Ref.
 16	454 (THF)	619.4 (THF) 624.4 (H ₂ O/THF)	0.018 (THF) 0.74 (H ₂ O/THF)	[48]
5-(4-Diphenylaminostyrene)barbituric acid	454 (THF)	633.4 (THF) 627.2 (H ₂ O/THF)	0.001 (THF) 0.032 (H ₂ O/THF)	[48]
 17	454 (THF)	633.4 (THF) 627.2 (H ₂ O/THF)	0.001 (THF) 0.032 (H ₂ O/THF)	[48]
5-(4-Diphenylaminostyrene)-1,3-dimethylbarbituric acid	454 (THF)	633.4 (THF) 627.2 (H ₂ O/THF)	0.001 (THF) 0.032 (H ₂ O/THF)	[48]
 18	360 (THF)	425, 530 (THF)	0.000013 (THF) 0.0039 (H ₂ O/THF)	[49]
4-(3-Benzo[d]thiazole-2-yl)-5-tert-butyl-4-hydroxybenzyl-2-(benzo[d]thiazol-2-yl)-6-tert-butylphenol	360 (THF)	425, 530 (THF)	0.000013 (THF) 0.0039 (H ₂ O/THF)	[49]
 19	267, 317 (THF)	420 (THF)	0.035 (THF) 0.054 (THF/H ₂ O = 1 : 9)	[50]
2-(3-(1H-Benzo[d]thiazol-2-ylthio)quinoline-ethanol	267, 317 (THF)	420 (THF)	0.035 (THF) 0.054 (THF/H ₂ O = 1 : 9)	[50]
 20	384, 485 monomer (DMF) 401, 519 aggregate (DMF)	617 (monomer) 637 (aggregate)	0.002 (DMF) 0.016 (aggregate)	[51]
2,4,6-Tri{(E)(4-ethoxyphenyl)-2,6-diethylphenyl}diazeny]benzene-1,3,5-triol	384, 485 monomer (DMF) 401, 519 aggregate (DMF)	617 (monomer) 637 (aggregate)	0.002 (DMF) 0.016 (aggregate)	[51]

Note. $\lambda_{\max}^{\text{abs}}$ is the position of the absorption band maximum, $\lambda_{\max}^{\text{fl}}$ is the position of the fluorescence band maximum, ϕ is the luminescence quantum yield.

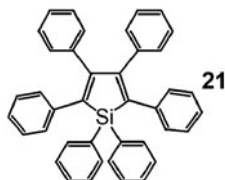
MECHANISMS OF AGGREGATION-INDUCED EMISSION

Several mechanisms have been put forward to explain aggregation-induced emission (AIE). In early reports, the mechanism of restricted intramolecular rotation (RIR) first proposed by Chen et al. [10] was popular. Other mechanisms based on restricted intramolecular vibrations (RIV) and intramolecular motion (RIM) [52] have also been proposed. In recent decades, mechanisms have also been proposed involving photoinduced electron transfer, intermolecular charge transfer, fluorescent inductive resonance energy transfer, charge transfer from ligands to metal, formation of excimers and exciplexes, as well as the abovementioned excited state intramolecular proton transfer (ESIPT). Realization of all these mechanisms reduces predominantly to hindrance to molecular motion such as rotation, vibration, and conformational change such that the nonradiative channels for the degradation of excitation energy is blocked and self-quenching is suppressed due to the effect of the medium (change in the nature of the solvent, viscosity, and temperature), which results in the formation of luminescent aggregates.

Hindrance to Intramolecular Rotation

The major structural feature of organic molecules, which demonstrate a unique improvement of emission in the solid state due to hindrance to intermolecular rotation, is the presence of fragments capable of rotation about C–C, C–N, or N–N single bonds. Nile red and carbocyanines are such molecules. Although only the contribution of intramolecular rotation is considered in explaining their optical properties, other types of motion such as vibrations including bending and twisting should also be taken into account since such motions use excited state energy [53].

Rotation about the C–C Bond. The mechanism based on hindrance to intramolecular rotation was first proposed by Chen et al. [11] on the basis of an analysis of the results of a study of a typical AIE fluorophore, namely, 1,1,2,3,4,5-hexaphenylsilol (**21**). The silol ring in this molecule is bonded to six phenyl rings by single bonds, which imparts conformational flexibility, and this molecule may take a propeller-like conformation [54]. As a consequence of a strongly twisted conformation due to the steric repulsion of adjacent phenyl groups, dense head-to-head packing of these molecules is impossible and there is no π – π stacking interaction in the solid state. However, C–H \cdots π interactions arise between molecules of **21** with short contacts (2.587–3.642 Å), which stabilize the crystal packing and restrict rotation of the phenyl groups [52].



Hexaphenylsilol **21** is highly soluble in organic solvents such as THF, chloroform, acetonitrile, and acetone, less soluble in methanol, and insoluble in water. Thus, water is used as a precipitating agent causing aggregation of molecules of **21** in solvents with added water such as in aqueous acetone. A dilute solution of **21** in acetone has a low fluorescence quantum yield ($\phi \approx 0.001$). The value of ϕ hardly changes as long as the water fraction in aqueous acetone does not exceed ~ 50 vol.%, but then steadily rises with increasing water fraction. When the water content is ~ 90 vol.%, the quantum yield rises to 0.22, which is ~ 220 times greater than the emission yield of a solution of **21** in pure acetone [11].

Similar trends in the change of luminescence properties were also found in solutions of **21** in aqueous THF (Fig. 4) with an increase in the emission quantum yield from 0.0015 in pure THF to 0.003, 0.35, 0.03, and 0.13 in mixtures with 60%, 70%, 80%, and 90% water, respectively. Bhongale et al. [55] have shown that the observed enhancement of fluorescence in solutions with different water content in H₂O/THF is related not only to the AIE effect but also depends on the structure morphology (nanocrystals, nanoglobules, and microglobules), which may form in these systems.

A study of the fluorescence of **21** in glycerol/methanol mixtures [11] showed that the emission intensity of this compound also is enhanced in solutions with higher viscosity. Thus, the emission intensity of **21** in 50 : 50 glycerol/methanol is

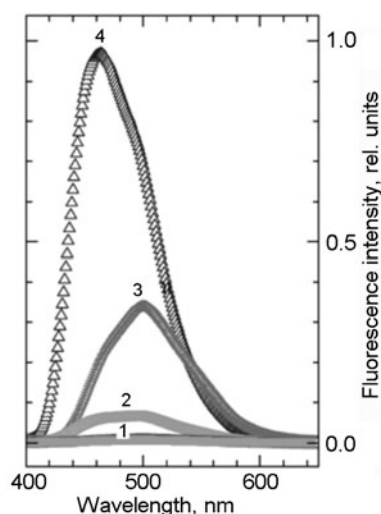
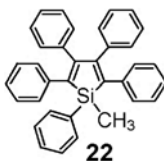


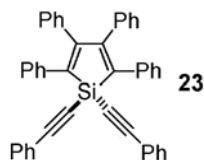
Fig. 4. Fluorescence spectra of **21** in aqueous THF with water content 0-60 (1), 80 (2) ($\lambda_{fl} = 485$ nm), 90 (3) ($\lambda_{fl} = 500$ nm), and 70 vol.% (4) ($\lambda_{fl} = 462$ nm). Reprinted with permission [55]. Copyright © 2006, Elsevier.

five times higher than in pure methanol. The greater viscosity of the solution restricts intramolecular rotation similar to cooling, which restricts thermoactivated intramolecular rotation [12].

An increase in the luminescence intensity of **21** and 1-methyl-1,2,3,4,5-pentaphenylsilol (**22**) with increasing aggregation of these compounds was also observed in aqueous ethanol solutions [10, 55]. In particular, the fluorescence quantum yield of **22** in 90 : 10 water/ethanol is 0.21, which is 333 times higher than in pure ethanol ($\phi = 0.63 \cdot 10^{-3}$).



Enhanced fluorescence intensity of a dioxane solution of 1,1-bis(phenylethynyl)-2,3,4,5-tetraphenylsilol (**23**) was observed with decreasing temperature due to hindrance to thermally activated intramolecular rotation (Fig. 5a) [11]. Cooling of a solution of this silol in THF to -196 °C led to an increase in the fluorescence intensity by a factor of ~ 360 in comparison with emission at room temperature (Fig. 5b). The effect of temperature on the fluorescence intensity of solutions of a series of other multiatomic heteroaromatic molecules was described in our previous work [56-58].



Similar to silol molecules, heterocyclopentadienyl derivatives such as 1,2,3,4,5-pentaphenylphosphole 1-oxide (**24**) [59], 1,2,3-triphenylphosphoindole 1-oxide (**25**), 1,2,3-triphenylphosphoindole (**26**) [60] also display change in the spectral luminescence properties upon variation of the ratio of the components in mixtures of organic solvents with water (Fig. 6). These three compounds have absorption bands with maxima in the near-UV region at 343 nm (**25**), 322 nm (**26**), and 386 nm (**24**). Weak emission with maxima at $\lambda_{fl} = 462$ and 423 nm and low quantum yields 0.0123 and 0.0134 is seen upon the photoexcitation of dilute solutions of **25** and **26** in THF, respectively. The emission maximum of **24** is even more strongly

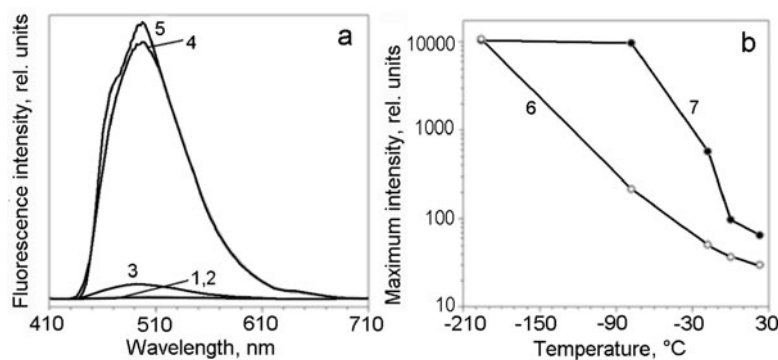


Fig. 5. a) Fluorescence spectra of **23** in 1,4-dioxane at 23 (1), 0 (2), -18 (3), -78 (4), and -96 °C (5); b) temperature dependence of the photoluminescence intensity of **23** in THF (6) and dioxane (7) ($C = 10 \mu\text{M}$, $\lambda_{\text{exc}} = 407 \text{ nm}$). Reprinted with permission [11]. Copyright © 2003, American Chemical Society.

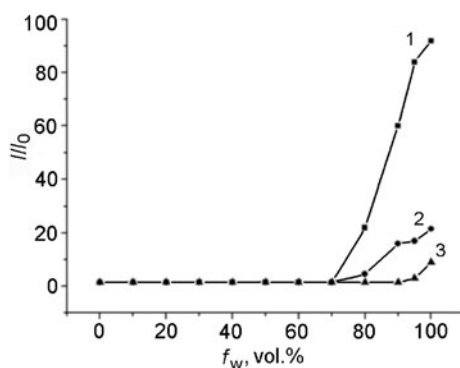
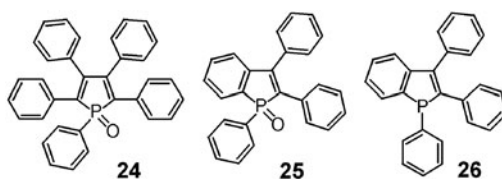
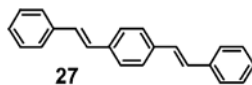


Fig. 6. Dependence of the relative fluorescence intensity of **24** (1), **26** (2), and **25** (3) on the water content (f_w) in aqueous acetonitrile [60].

shifted toward the red region ($\lambda_{\text{fl}} = 527 \text{ nm}$), while the fluorescence quantum yield is 0.0028. Thus, **25**, **26**, and **24** are extremely weak emitters in molecular-dissolved state. The peripheral rings in **25**, **26**, and **24** can rotate in solution, rapidly losing excited state energy, which accounts for their low fluorescence quantum yields. When a large amount of water, in which these luminophores are insoluble, is added to solutions of **25**, **26**, and **24** in acetonitrile, their emission increases with increasing water content. In the solid state, **25** emits at $\lambda_{\text{fl}} = 478 \text{ nm}$ (quantum yield $\phi = 0.68$), the emission maximum of **26** is at $\lambda_{\text{fl}} = 469 \text{ nm}$ ($\phi = 0.1$), while the fluorescence band of **24** is at $\lambda_{\text{fl}} = 532 \text{ nm}$ ($\phi = 0.33$).



The fluorescence of crystals of distyrylbenzene (**27**) [61] and also its submonolayers on aluminum oxide and silica obtained by adsorption of solutions of **27** was studied by Egelhaaf et al. [62]. Upon the maturation of films consisting of several monolayers, enhancement of fluorescence intensity due to the aggregation of monomers was observed (Fig. 7).



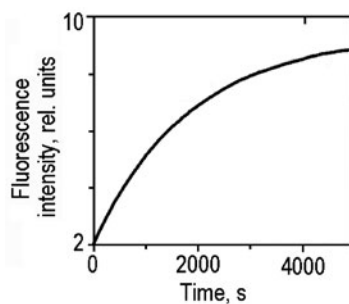


Fig. 7. Increase in the fluorescence intensity over time of several multilayers of **27** on fused silica. Reprinted with permission [62]. Copyright © 1992, Elsevier.

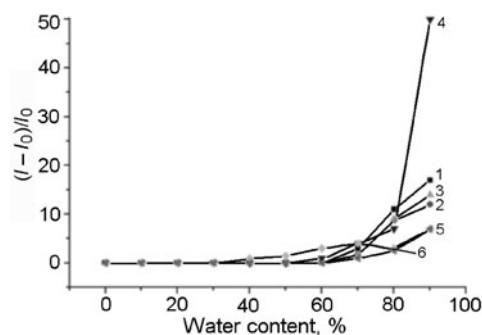
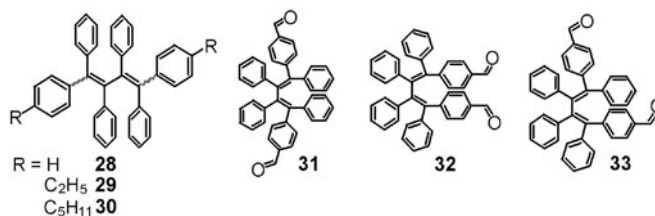


Fig. 8. Dependence of the relative fluorescence intensity of solutions of **30** (1), **29** (2), **28** (3), **31** (4), **32** (5), and **33** (6) on the water content in aqueous THF [63, 64].

Zhang et al. [63, 64] studied a series of AIE-active dyes, namely, hexaphenyl-1,3-butadienes **28-33**. The fluorescence intensity of these compounds in solutions with water content less than 60% in aqueous tetrahydrofuran is negligible (Fig. 8), which is attributed to nonradiative deactivation of excitation due to free intramolecular rotation around the σ -bonds between the phenyl and alkenyl groups. The emission intensity sharply increases when the water fraction reaches 70%, which corresponds to the formation of aggregates of **28**, **29**, and **30** with mean particle diameter 330, 303, and 234 nm, respectively [63]. Aggregates of **31** (mean particle diameter 64-67 nm), **32** (144 nm), and **33** (125 nm) are formed when the water fraction is 90% [64]. The aggregates in the mixed aqueous THF solvents are in an amorphous state and/or exist as a mixture of amorphous and crystalline formations. The emission quantum yields of **28** in the crystalline and amorphous states are 0.0353 and 0.0242, respectively. This discrepancy indicates that the more compact crystalline aggregates are better luminophores. The quantum yield in the solid state for **31** $\phi = 6.74\%$ ($\lambda_{\max} = 553$ nm), **32** $\phi = 7.24\%$ ($\lambda_{\max} = 510$ nm), and **33** $\phi = 5.57\%$ ($\lambda_{\max} = 537$ nm) [64]. The fluorescence increases sharply with increasing water content up to 90% in aqueous THF: by factors of 14, 12, and 17 for **28**, **29**, and **30**, respectively, by a factor of 50 for **31** and by a factor of 7 for **32**.



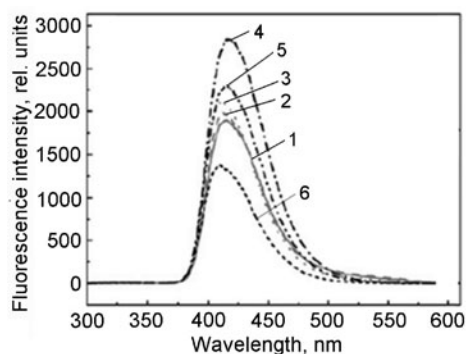
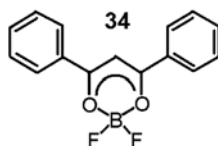
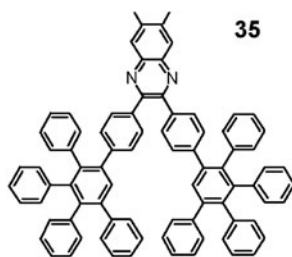


Fig. 9. Fluorescence spectra of **35** in THF–water mixtures with component ratios (%) ($\lambda_{\text{exc}} = 280 \text{ nm}$, $C = 9 \cdot 10^{-6} \text{ M}$) 2/98 (1), 10/90 (2), 25/75 (3), 50/50 (4), 75/25 (5), and 100/0 (6). Reprinted with permission [67]. Copyright © 2008. The Royal Society of Chemistry.

In the case of a difluoroborate derivative with a dibenzoylmethane fragment (**34**) in a matrix of polymethyl methacrylate, the capacity to produce AIE was established by measuring the changes in the luminescence spectra of monomer form of **34** upon the addition of water to its solution in acetone [65, 66]. The extent of aggregation of the luminophore increases in the presence of water. The intensity of the monomer fluorescence with maximum at $\lambda_{\text{fl}} = 420 \text{ nm}$ increases in the first stage of this process. The greater aggregation is manifest also in the increase of lifetime of the excited state of **34** from 0.5 to 2.4 ns. The emission lifetime of the excited monomer form of **34** in the polymer matrix is somewhat greater (0.61 ns) in comparison with solution, which is attributed to a decrease in the probability of nonradiative processes. The longer-lived emission, whose contribution increases with increasing recording wavelength, is related to the luminescence of excimers. Still another process with $\tau = 3.5 \text{ ns}$ and $\lambda_{\text{fl}} = 445 \text{ nm}$ is attributed to AIE [65, 66].



Nanoparticles of 6,7-dimethyl-2,3-di(4-(2,3,4,5-tetraphenylphenyl)phenyl)quinoxaline (**35**), which is a polyphenyl-phenyldendron, display sensitivity toward nucleic bases in aqueous solutions and are hence used to determine these bases [67]. Derivative **35** fluoresces in THF with maximum at 412 nm. In contrast to many AIE luminogens, the emission of **35** in aqueous THF does not change with increasing concentrations of this compound in solution. This finding may be the result of a combination of effects: intramolecular rotation, intermolecular hydrogen bonding, solvent viscosity, and hydration. Furthermore, the formation of nanoparticles of **35** with mean diameter 165 nm is observed in aqueous solutions. Due to the aggregation of **35** in aqueous tetrahydrofuran mixtures, when the water fraction increases from 0% to 50%, hindrance to intramolecular rotation in these molecules leads to a two-fold increase in the emission and a slight shift in the emission maximum toward the red region by 4-6 nm ($\lambda_{\text{fl}} = 420 \text{ nm}$) (Fig. 9).



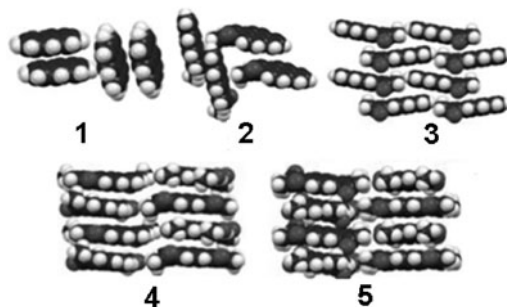
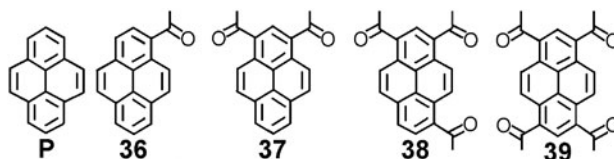


Fig 10. Structures of aggregates of pyrene and its derivatives **36-39** in the crystalline state: pyrene (**1**, sandwich herringbone structure, $\rho = 3.40$), **33** (**2**, herringbone structure, $\rho = 19.54$), **37** (**3**, sheet-like π - π stacking structure, $\rho = 2.56$), **38** (**4**, column π - π stacking structure, $\rho = 0.89$), **39** (**5**, column π - π stacking structure, $\rho = 0.46$) (ρ is the ratio of C \cdots H and C \cdots C interactions in the crystal, %). Reprinted with permission [68]. Copyright © 2014, The Royal Society of Chemistry.

Rajagopal et al. studied the effect of the acylation [68] and benzylation [69] of pyrene (P) on the crystal structure of **36-39**. The acylation of pyrene is accompanied by a considerable decrease in the interplane angle between adjacent units in the crystal of **36** ($\theta = 48.4^\circ$) and **39** ($\theta = 0^\circ$). The decrease in the interplane angle leads to transformation of the herringbone structure in **36** into the columnar structure in **39** (Fig. 10).



An increase in the number of acetyl groups in chloroform solution leads to a bathochromic shift of the absorption maximum of **36-39**, in particular, by 22 nm for **36** ($\lambda_{\text{abs}} = 359$ nm) and by 70 nm for **39** ($\lambda_{\text{abs}} = 407$ nm) relative to the absorption of pyrene ($\lambda_{\text{abs}} = 337$ nm). The emission band maxima of its acyl derivatives in this solvent also undergo a bathochromic shift with a significant decrease in the fluorescence quantum yield: $\lambda_{\text{fl}} = 412$ nm, $\phi = 0.004$ for **36** and $\lambda_{\text{fl}} = 435, 535$ nm, $\phi = 0.002$ for **37** relative to the emission of P ($\lambda_{\text{fl}} = 393$ nm, $\phi = 0.75$).

Derivatives **36-39** in the crystalline state all display a red shift in their spectra relative to the position of the absorption bands and emission of pyrene $\lambda_{\text{abs}} = 386$ nm, $\lambda_{\text{fl}} = 472$ nm ($\phi = 0.071$). Thus, in the case of **39**, $\lambda_{\text{abs}} = 486$ nm and $\lambda_{\text{fl}} = 646$ nm ($\phi = 0.071$). The red shift of the excimer-like fluorescence structures of **36-39** was related to the combination of additional conjugation involving the acetyl groups and increased overlap between adjacent pyrene fragments. An enhanced fluorescence quantum yield in the crystalline state is observed for all derivatives **36-39**. The highest quantum yields found for **37** ($\phi = 0.325$) and **38** ($\phi = 0.277$) were related to the formation of J-aggregates [68].

Along with the acylation of pyrene, the benzylation of this compound also leads to the formation of luminescent green-yellow-orange crystals. AIE arises in **40-43** due to restricted rotational motion of the benzoyl groups and the lack of solvation in the crystalline state, which is supported by the finding of greater fluorescence quantum yields of crystalline **40-43** ($\phi \approx 0.02-0.26$) than for solutions of these compounds ($\phi \leq 0.01$) (Fig. 11a). The benzoylpyrene derivatives have broad colored gamma emission, which is used in light emitting devices [69].

An increase in the number of benzoyl groups leads to a red shift in the absorption spectra, for example, by 114 nm (**40**) and by 60 nm (**43**) in comparison with crystalline P. Upon excitation at 380 nm, **40** exhibits a broad emission band with

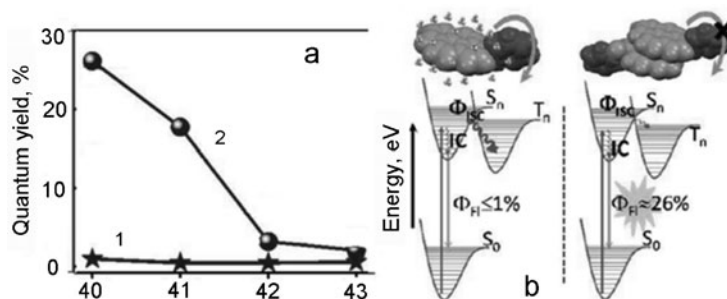
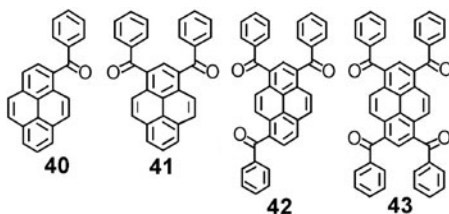
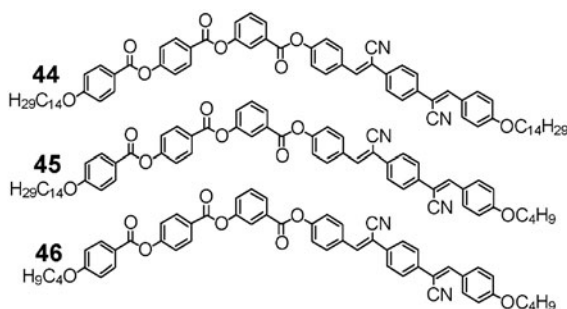


Fig. 11. a) Fluorescence quantum yield of **40-43** in solution (1) and in the crystalline state (2); b) Jablonski diagram representing the energy levels for **40** in solution (left) and the aggregate of **40** in the crystal (right). Reprinted with permission [69]. Copyright © 2016, The Royal Society of Chemistry.

maximum at $\lambda_{fl} = 620$ nm with a bathochromic shift of 148 nm relative to the emission maximum of crystalline pyrene. The increasing number of benzoyl groups in the series **41-43** is accompanied by a blue shift of the emission maximum relative to the emission spectrum of **40**. The observed differences in the position of the emission band maxima for **40-43** may be consequences of different extents of π - π overlap and distance between the molecular planes of adjacent pyrene units. The difference in energies between the S_1 and T_1 states in the monomer and dimer of **40** is 1.18 and 0.94 eV, respectively. The low fluorescence quantum yield of solutions of **40** may be a consequence of efficient intersystem crossing conversion (ISC) due to strong mixing of almost degenerate singlet and triplet states (Fig. 11b).



The spectra of dilute solutions of the twisted structures of dicyanodistyrylbenzene derivatives **44**, **45**, and **46** with various terminal alkoxy substituents (*para*-tetradecyloxy or *para*-butoxy groups) in dichloromethane (DCM) show absorption bands at about 270 and 372 nm due to the polybenzoate and distyrylbenzene chromophores as well as a weak luminescence band with maximum $\lambda_{fl} = 455$ nm ($\phi = 0.002$). The emission band maxima of solid solutions of these compounds in PMMA films are shifted toward the blue region to $\lambda_{fl} = 440$ nm, while the emission quantum yield rises to $\phi = 0.04$. The emission bands of powders of **44**, **45**, and **46** are found at longer wavelengths ($\lambda_{fl} = 573$ -588 nm) in comparison with solution. Martinez-Abadia et al. [33] reported that the quantum yields of the powders are higher than in solution in DCM and similar to the emission yields of solid solutions in PMMA ($\phi = 0.04$ -0.06). However, considering the values given for nonradiative degradation ($6.6 \cdot 10^{-7}$ s)



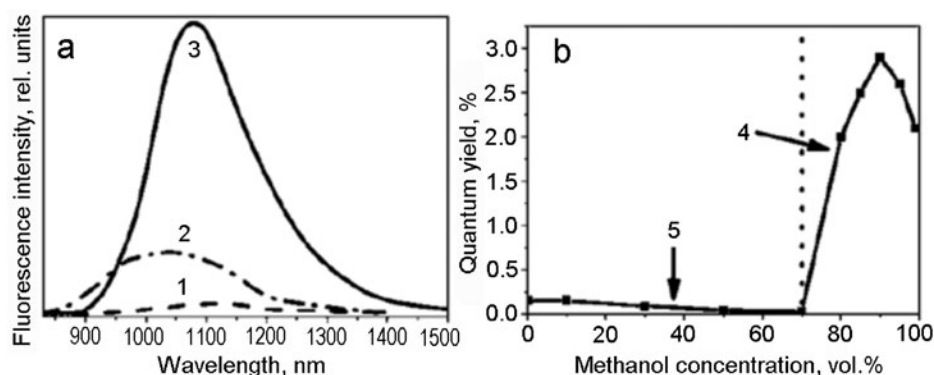
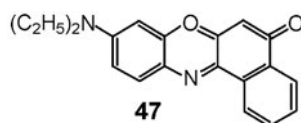


Fig. 12. a) Fluorescence spectra of **48** in THF solution (1), in 1 : 9 (vol.) THF/CH₃OH (2), and in a film (3) ($C = 10 \mu\text{M}$, $\lambda_{\text{exc}} = 700 \text{ nm}$ (for solution), 694 nm (for film)); b) dependence of the quantum yield of **48** on the composition of the THF/CH₃OH mixture: 5) isolated particles. Reprinted with permission [72]. Copyright © 2008, American Chemical Society.

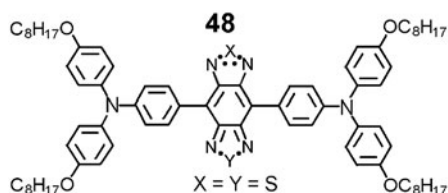
and radiation velocity ($4.2 \cdot 10^{-6} \text{ s}$), the emission quantum yield of the powders is 0.88. Such effects are also characteristic for α -cyanostilbenes and have been attributed to the effect of the rigidity of the medium, which restricts nonradiative deactivation involving rotation. Molecules of similar donor–acceptor structure **10** and **11** shown in Table 1 have emission characteristics typical for induced aggregation (high quantum yield and practical lack of fluorescence in solution).

Rotation around the C–N Bond. The effect of enhanced emission in the solid state due to restricted intramolecular rotation around the C–N bond is characteristic for Nile Red (**47**), which is one of the best known highly fluorescent dyes with pronounced solvatofluorochromic properties; the quantum yield of **47** varies from 0.57 in ethanol to ~ 0.7 in other solvents. Strong quenching of the emission of **47** ($\phi = 0.018$) is observed in media containing water [70].

In order to study the AIE effect, nanoparticles of **47** were encapsulated in pure silica obtained by the hydrolysis of tetramethyl orthosilicate and into hybrid sol–gel matrices obtained from glycidoxypropyltrimethoxysilane. Increasing the concentration of **47** from $3 \cdot 10^{-5}$ to $1.5 \cdot 10^{-3} \text{ mmol/L}$ in the silica samples leads to the formation of nonfluorescent sandwich-type aggregates and an increase in the fluorescence intensity is noted in the hybrid glasses by a factor of 525 in comparison with the emission of **47** in SiO₂ matrices [71].



The dye 4,8-bis[4-(N,N-bis(4-octyloxyphenyl)amino)phenyl]benzo[1,2-c:4,5-c']bis([1,2,5]thiadiazole) (**48**) in the solid state shows an AIE effect in the near-IR spectral region ($\lambda_{\text{fl}} = 1078 \text{ nm}$) (Fig. 12a) [72]. The absorption maximum and luminescence bands of **48** in toluene are at $\lambda_{\text{abs}} = 763 \text{ nm}$ and $\lambda_{\text{fl}} = 1065 \text{ nm}$; the emission quantum yield $\phi = 0.071$. Upon the addition of methanol (up to 70 vol.%) to a solution of **48** in THF, the fluorescence quantum yield ($\phi \approx 0.001$) remains virtually invariant and then increases sharply to $\phi \approx 0.29$ at methanol concentration 90 vol.% in the solvent mixture (Fig. 12b). Qian et al. [72] suggested that the AIE phenomenon in **48** is related to a mechanism of restricted intramolecular vibrational and rotational motions in the solid state.



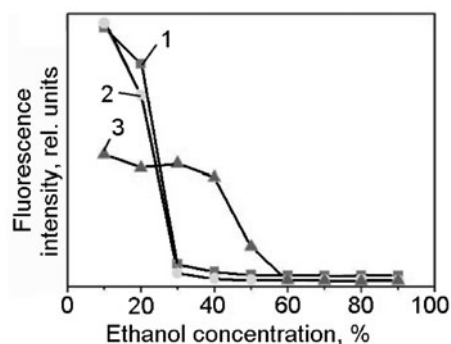
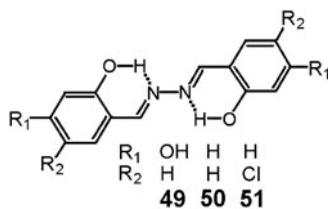


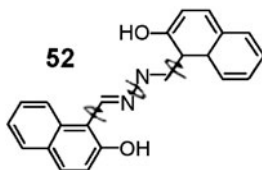
Fig. 13. Effect of the volumetric fraction of ethanol on the fluorescence intensity of azine derivatives **49** (1), **50** (2), and **51** (3) in aqueous ethanol ($\lambda_{\text{exc}} = 400$ nm). Reprinted with permission [73]. Copyright © 2009, American Chemical Society.

Rotation around the N–N Bond. An AIE effect is observed in a series of salicylaldehyde azine derivatives [73], in which the salicylaldehyde parts are attached to each other by means of an N–N single bond. Intramolecular hydrogen bonds permit rotation only around the N–N bond. Solutions of 4-hydroxysalicylaldehyde azine (**49**), salicylaldehyde azine (**50**), and 5-chlorosalicylaldehyde azine (**51**) in 9 : 1 ethanol/water have structured bands in their absorption spectra and weak fluorescence. Enhanced intensity of the absorption band in the long-wavelength spectral region and the appearance of fluorescence are observed in 1 : 9 ethanol/water (Fig. 13). Increased luminescence of these compounds was also found in a viscous glycol/glycerol solvent. The emission quantum yields of **49-51** in solution are 0.002, 0.002, and 0.001, respectively, while these values in the aggregated state are 0.13 ($\tau = 3.09$ ns), 0.11 ($\tau = 3.05$ ns), and 0.05 ($\tau = 2.32$ ns), respectively.

Figure 13 shows that the onset of the AIE effect is seen at 30 vol.% ethanol for **49** and **50** and 60 vol.% for **51**. Salicylaldehyde azine (**50**), which is a symmetrical Schiff base, has weak emission ($\phi = 0.002$) in ethanol solution but its luminescence increases upon the addition of water, which facilitates the formation of aggregates. Tang et al. [73] assumed that the hydroxyl groups of the ethanol solvent molecules compete with the hydroxyl groups of **50** in the formation of intermolecular hydrogen bonds, which is not quite in accord with the proposed mechanism since there are also hydroxyl groups in water molecules and intermolecular hydroxyl bonds may be formed with **50**.



AIE properties are also characteristic for 2-(1-hydroxy-2-naphthyl)methylenehydrazone (**52**). The luminescence intensity of this compound increases significantly upon the addition of water to its solution in DMF (Fig. 14). The emission quantum yields of **52** in pure DMF and in the aggregated state are 0.057 and 0.27, respectively [74].



The AIE effect is also characteristic for azines **53-55**, which contain various groups, including 4-methylcoumarin, in which intramolecular proton transfer is possible in the excited state [75]. The emission quantum yields of these compounds in

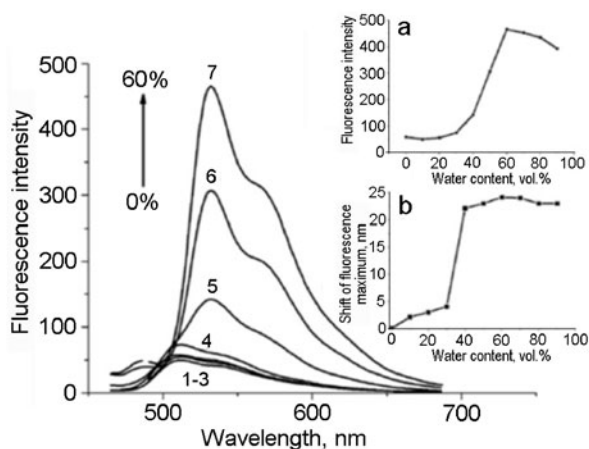
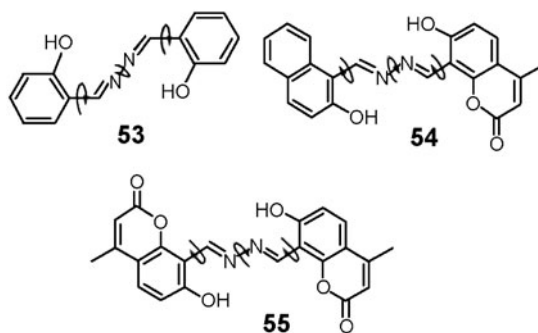
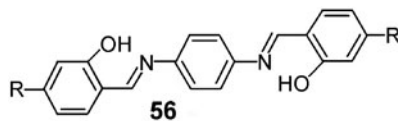


Fig. 14. Change in the fluorescence intensity of **52** with increasing water fraction in aqueous DMF: 1) 0, 2) 10, 3) 20, 4) 30, 5) 40, 6) 50, 7) 60 vol.%. Inserts: a) change in the integral fluorescence intensity of **52** with increasing water content in aqueous DMF, b) change in the position of the fluorescence maximum of **52** with increasing water content. Reprinted with permission [74]. Copyright © 2013, Elsevier.

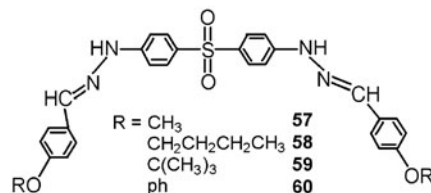
the aggregate state are 0.55 and 0.83, respectively, while their solutions in dimethyl sulfoxide (DMSO) hardly fluoresce. In the isolated state, the mobile units in these luminogen molecules rotate around the C–C and N–N bonds of the enol form or the C–C, N–N, and C–N bonds of the ketone form, quenching the energy of the excited state and facilitating nonradiative relaxation. The molecules “freeze up” in the aggregate or solid state, which restricts intramolecular motion thereby facilitating radiative deactivation of photoexcitation. Thus, the introduction of various groups from phenyl and naphthyl groups to the 4-methylcoumarin group permits us to alter the luminescence color of the resultant luminophores from green (**53**) to yellow (**52**), orange (**54**), or red (**55**).



Derivatives of *N,N'*-bis(salicylidene)-*p*-phenylenediamine (**56**) also display AIE. These compounds have very weak luminescence in THF solution but strongly emit upon aggregation in aqueous THF with 90 vol.% water. The emission quantum yield of these compounds in aqueous THF with 90 vol.% water ($\lambda_{\text{exc}} = 360 \text{ nm}$) is 0.33 for R = H (**9**), 0.08 for R = Me (**56**), and 0.12 for R = OMe (**56**), which is greater than in pure THF by factors of 400, 80, and 18, respectively [76].

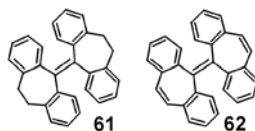


Similar changes in spectral luminescence properties in going from solutions in pure THF to aqueous THF were found for the series of *bis*-4,4'-di(E)-2-(4-4-alkoxyaniline)hydrazinyldiphenyl sulfones (D- π -A- π -D) [77]. The emission quantum yields of these compounds in aqueous THF are greater than in THF solution; the enhancement is from 0.004 to 0.027 for R = CH₃ (**57**), from 0.0003 to 0.069 for R = -CH₂-CH₂-CH₂-CH₃ (**58**), from 0.0003 to 0.057 for R = -C(CH₃)₃ (**59**), and from 0.0016 to 0.22 for R = Ph (**60**). The formation of aggregates due to intermolecular hydrogen bonding between adjacent molecules, which restricts intramolecular rotation, leads to enhancement of AIE.



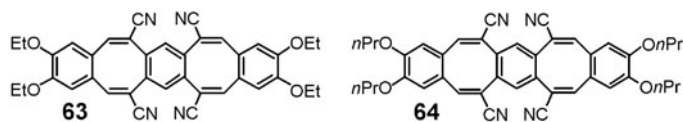
Restriction to Intramolecular Vibrations

Studies of AIE-luminophores have shown that some of these molecules lack rotating fragments. Thus, the appearance of AIE for such molecules cannot be explained by the RIR mechanism but may be described satisfactorily by the RIV mechanism. Examples of such compounds are 10,10',11,11'-tetrahydro-5,5'-bidibenzo[a,d][7]annulenyldiene (**61**) and 5,5'-bidibenzo[a,d][7]annulenyldiene (**62**) [78]. The emission spectrum of **61** has maximum at 380 nm in aggregation state; its quantum yield is 0.23. Compound **62** emits at a longer wavelength (395 nm) with quantum yield 0.3. Solutions of these compounds have very weak emission with quantum yield 0.001 and 0.005, respectively.



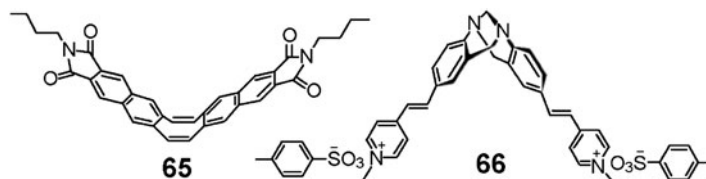
The results of computer modelling carried out using the hybrid QM/MM method combining molecular mechanics and quantum mechanics procedures showed that an isolated molecule of **61** has six normal vibrational modes, which consume a considerable amount of excited state energy (the reorganization energy of each mode >200 cm⁻¹, which leads to a total energy loss of 5679 cm⁻¹). For comparison, **61** in a cluster has only three normal modes, which consume a much smaller amount of excitation energy (~4016 cm⁻¹). In this case, the combination of a reduced number of normal vibrational modes and the loss of ~30% of the exciton energy due to intramolecular vibrations permits deactivation of the excited state of **61** through a radiative channel, which leads to the observed AIE effect [78, 79].

The RIV mechanism responsible for the AIE effect has been proposed in a study of a series of π -systems containing flexible cyclooctatetraene (COT) rings [80]. Such AIE phosphores consist of three benzene blocks connected by two COT rings. Conformational changes of the COT rings in these molecules permit structural flexibility. In solution, these compounds may undergo various vibrational inversions, leading to the formation of boat-boat, boat-chair, and chair-chair conformations. Such intramolecular vibrations lead to nonradiative loss of excitation energy such that solutions of these compounds do not fluoresce. In the crystalline state, conformational changes of the COT rings are restricted by intermolecular interactions and steric packing effects, restricting intramolecular vibrations. The nonplanar molecular structure also restricts intermolecular π - π stacking interactions. Together these effects lead to the appearance of luminescence in crystals of these compounds. Although they fluoresce only weakly, their solvated monocrystals emit at 450-500 nm. The emission quantum yields of these structures in the case of **63** in CHCl₃, **64** in CH₂Cl₂, and **64** are 0.038, 0.06, and 0.071, respectively, which is greater than in their solutions by factors of 380, 600, and 710, respectively. Compounds **63** and **64** form powders in the solid state, which have very weak emission due to vibration of the COT ring.



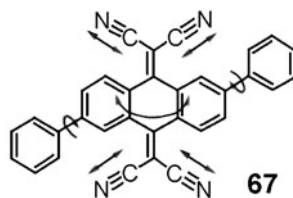
Molecules consisting of a flexible COT ring connecting two N-arylimide groups through phenyl, naphthyl (**65**), and anthracene units are also AIE-luminogens [81], as indicated by the lack of emission in ordinary solvents and the appearance of strong fluorescence in the aggregate state at a band with maximum 412 nm with quantum yield 0.17. Enhancement of fluorescence intensity is also observed upon cooling a solution of **65** in 2-methyltetrahydrofuran from 296 to 103 K with a hypsochromic shift of the emission maximum to 393 nm.

Another flexible molecule, 2,8-(6H,12H-5,11-methanodibenzo[b,f]diazacylidene)-di(*p*-ethenyl-N-methylpyridinium) ditosylate (**66**) is also a typical AIE luminogen [82]. Ditosylate (**66**) consists of a V-shaped unit with styrylpyridinium blocks on each side, which are reminiscent of stilbene structure. The fluorescence spectrum of **66** extends to 510 nm and has a maximum at 400 nm, while a band with maximum at $\lambda_{fl} = 550$ nm is observed in acetonitrile–toluene. The intensity of this band increases by a factor of 225 with increasing toluene fraction up to 98% due to the formation of aggregates.

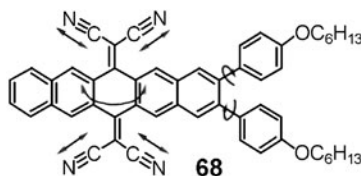


Restriction to Intramolecular Motion

This mechanism is used to explain the AIE effect in compounds, in which it is impossible to clearly distinguish between rotational and vibrational motions. An example is 11,11,12,12-tetracyano-(2,6-diphenyl)-9,10-anthraquinodimethane (**67**), in which the central unit is connected to two phenyl rings at C-2 and C-6. This compound does not luminesce in acetonitrile and upon the addition of a small amount of water. Enhanced emission by a factor of 33 is observed when the water content exceeds 60% [83].



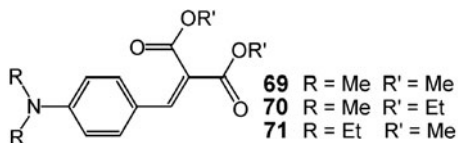
Tetracyano derivative **68**, in which the pentacenequinodimethane unit is attached to identical phenyl groups, is a structure also possessing AIE luminogen properties. This compound does not fluoresce in THF solution but emits in aqueous THF with water content about 70 vol.%, which favors the formation of luminescing nanoaggregates [84, 85].



The low luminescence quantum yield of a solution of 1,4-bis(((9H-carbazol-9-yl)phenyl)ethynyl)benzene (**13**) in THF (see Table 1) is attributed to very rapid motions, including rotation and/or vibration of several molecular fragments, which facilitates efficient nonradiative excitation energy degradation. On the other hand, crystallization of this derivative decreases the frequency of molecular motions, leading to the observed enhanced emission in the solid state [47].

4-Dialkylamino-2-benzylidenemalononic acid esters **69–71** in dilute toluene solution have hardly detectable emission ($\phi \approx 0.001$) with bands at $\lambda_{fl} = 429$ nm (**69**) and $\lambda_{fl} = 440$ nm (**70**) [86] but fluoresce with higher quantum yields up to $\phi \approx 0.38$ as powders. A significant red shift of the emission bands to 468 and 473 nm is observed. A significant increase in the quantum

yield of **69** from 0.001 to 0.026 was noted in going from THF to a more viscous solvent, namely, polyethylene glycol. Enhanced emission is also seen when water is added to a methanol of **69** when the water content is above 50 vol.%, which leads to aggregation of its molecules to give pseudonanoclusters with stronger luminescence.



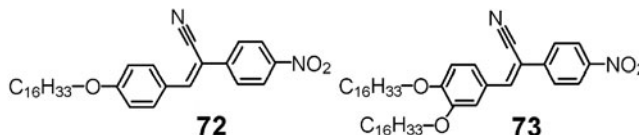
Crystalline films of **69** have bright blue emission with maximum at $\lambda_{fl} = 468$ nm and quantum yield 0.38. In contrast, its amorphous films demonstrate only weak blue-green fluorescence ($\lambda_{fl} = 500$ nm) at room temperature with quantum yield 0.01. The lowest quantum yield ($\phi \approx 0.003$) was found for **69** in polymethyl methacrylate (PMMA). We should note that the fluorescence intensity is significantly higher with decreasing temperature of a solution of **69** and upon cooling a PMMA film containing **69** [86]. The relatively weak fluorescence of a methanolic solution of **69** and its stronger emission in the crystal are in accord with the results of TD-DFT, CASSCF, and ONIOM (QM : MM) quantum-chemical calculations [87].

Fluorescent Properties of Aggregates of J-Type Molecules

An explanation of how molecular packing affects the photophysical properties of aggregates was proposed more than five decades ago by M. Kasha [88], who showed that the coulombic interaction between two molecules induces spectral shifts of the absorption bands and leads to change in the radiative degradation of the excitation of such molecules in comparison with the free molecules. In J-aggregates, dipole moments line up from head to tail, which leads to a bathochromic shift of the absorption bands and enhancement of the rate of radiative degradation of excitation energy [88]. J-Aggregates are building blocks in the formation of nanoparticles and thus determine the efficiency of their fluorescence [35, 89-91]. J-Aggregates, in which molecules are arranged head-to-tail, specifically tend to have relatively high fluorescence efficiency [92, 93]. A number of authors [89, 94-96] have assumed that the structure of crystals of organic compounds consisting of J-aggregates determines their photooptical properties.

Shapiro et al. [97] studied meso-alkyl-substituted thiocarbocyanine dyes and found that the ethyl group, as a rule, facilitates the formation of J-aggregates in aqueous solution, while the methyl group facilitates the formation of various types of H*-aggregates. The introduction of the multicharged Eu^{3+} cation into aqueous solutions of these dyes shifts the equilibrium toward aggregates: the meso- CH_3 -substituted dyes form mostly H*-aggregates, while meso- C_2H_5 -substituted dyes form mostly J-aggregates. Thus, the alkyl group in the meso position relative to the polymethine chain in thiocarbocyanines acts as a regulator in the aggregation process due to stereochemical effects and dictates the morphology and spectral properties of the resultant aggregate [97].

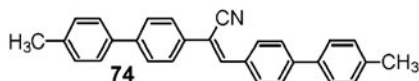
Examples of compounds displaying enhanced fluorescence due to the formation of J-aggregates during the sol-gel phase transformation are (Z)-3-(4-(hexadecyloxy)phenyl)-2-(4-nitrophenyl)acrylonitrile (**72**) and (Z)-3-(3,4-bis(hexadecyloxy)phenyl)-2-(4-nitrophenyl)acrylonitrile (**73**) [30], which fluoresce in pure THF with quantum yield ~ 0.005 . Both these compounds gelatinize in aqueous THF and in DMSO, while **73** forms a gel upon ultrasonic treatment also in acetone with enhancement of the fluorescence by a factor of 70.



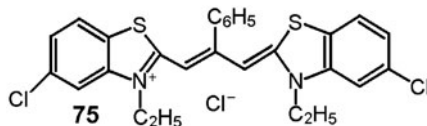
A significant increase in the emission intensity of these compounds was also observed upon decreasing the temperature. Thus, upon cooling a solution of **72** in DMSO from 100 °C to room temperature gives a hypsochromic shift of the emission maximum from 550 to 525 nm and a 20-fold increase in emission intensity. The fluorescence of a solution of **72** in

aqueous THF at 60 °C is very weak. Upon cooling this solution, the fluorescence band maximum shifts from 535 to 525 nm and its intensity increases by a factor of 40 in comparison with the hot solution in aqueous THF and a factor of 90 relative to a solution of the same concentration in pure THF. In the case of **73**, the weak emission band at $\lambda_{fl} = 540$ nm for this compound in aqueous THF at 60 °C undergoes a bathochromic shift to 574 nm upon cooling the solution to room temperature, which is accompanied by a seven-fold increase in the emission intensity.

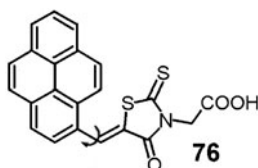
An effect of aggregation on emission is also found for cyanostilbenes [31], which are linear π -conjugated organic luminophores. Liu et al. [18] attributed the changes in the spectral luminescence properties of 1-cyano-*trans*-1,2-*bis*(4'-methylbiphenyl)ethylene (**74**) to intra- and intermolecular interactions. Isolated molecules of **74** in aqueous THF with water content up to 50% hardly fluoresce ($\phi \approx 0.001$). The emission quantum yield is enhanced when there is 60 vol.% water in the solvent mixtures and spherical nanoparticles of **74** begin to form with mean diameter 30-40 nm. When the water content is 80%, the fluorescence quantum yield is enhanced by a factor of almost 700 ($\phi = 0.69$) relative to the emission quantum yield of **74** in pure THF and there is a bathochromic shift of the emission band from $\lambda_{fl} = 455$ nm to $\lambda_{fl} = 488$ nm. The enhancement of the fluorescence of nanoparticles of **74** is attributed to the synergistic effect of planarization and J-aggregation [98]. Semiempirical AM1 calculations supported the hypothesis that aggregation facilitates flattening the plane of molecules of **74**, favors expansion of the effective length of the conjugation chain, and enhances the oscillator strength of this molecule.



Enhancement of emission when the formation of J-aggregates is possible was observed in a study of the properties of 3,3'-diethyl-5,5'-dichloro-9-phenylthiacarbocyanine (**75**) [99]. The spectra of **75** in methanol show absorption bands with maxima at 528 and 566 nm with emission quantum yield $\phi \approx 0.015$. The addition of aqueous KCl to a methanolic solution of this dye, i.e., when conditions are created for the formation of J-aggregates, the absorption spectrum retains the monomer band at 566 nm but a new band appears at 673 nm related to absorption of the J-aggregate of **75**. The emission spectrum also has two bands: a band at 673 nm related to the J-aggregates and a band at 578 nm, which corresponds to monomer forms of the fluorophore. The fluorescence quantum yield of the monomer taken in aqueous solution as unity is 0.015 in methanol. Upon excitation at $\lambda = 575$ nm, the quantum yield is increased by a factor of 10, while upon excitation at $\lambda = 615$ nm, the yield is enhanced by a factor of 22.



An AIE effect has been described for a pyrene derivative of rhodaninacetic acid (**76**), which is an organic donor-acceptor compound capable of forming particles with mean diameter 50-60 nm with strong red emission [100]. The absorption spectrum of **76** in methanol has a band at 333 nm typical for pyrenes and a charge transfer band at 442 nm. The charge transfer band is shifted to 502 nm upon the addition of water to a methanolic solution of **76**, which is ascribed to greater



effective length of the conjugation chain due to planarization of the molecule induced by aggregation, along with the appearance of a shoulder at 531 nm attributed to the formation of J-aggregates. The fluorescence spectrum of **76** in methanol has a band at 542 nm, which undergoes a bathochromic shift to 628 nm ($\Delta\lambda = 86$ nm) in 9 : 1 water-methanol due to the

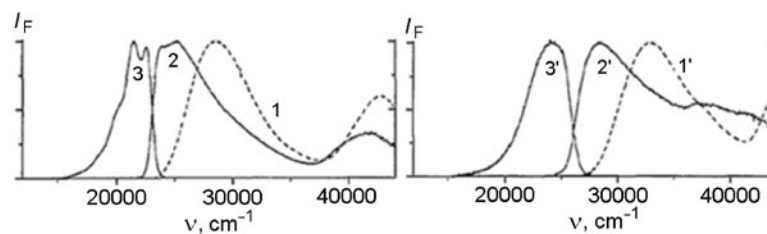
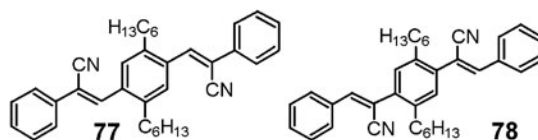


Fig. 15. Absorption spectra of solutions in dichloromethane (1, 1'), fluorescence excitation spectra (2, 2'), and fluorescence spectra (3, 3') of nanoaggregates or microcrystals of **77** (1, 2, 3) and **78** (1', 2', 3'). Reprinted with permission [102]. Copyright © 1996, Elsevier.

formation of nanoparticles of this molecule. Quantitative evaluation of the ratio of the fluorescence intensities of solutions in methanol and water–methanol showed that the emission intensity of the mixed solution increases by a factor of 4–40 with increasing water volumetric fraction to 70%–90%. The luminescence quantum yield of the methanolic solution of **76** is extremely low ($\phi = 0.004$) but increasing the water fraction to 90 vol.%, which facilitates the formation of nanoparticles of this molecule, enhances this value to $\phi = 0.180$ [100].

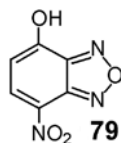
Benzene derivatives 1,4-*bis*(α' -cyanostyryl)-2,5-di-*para*-hexylbenzene (**77**) and 1,4-*bis*(β -cyanostyryl)-2,5-di-*para*-hexylbenzene (**78**) are clear examples of rod-like π -conjugated molecules, which form a family of phenylenevinylene derivatives [34]. Most of these compounds fluoresce in solution with high quantum yield close to unity [101]. Oligophenylenevinylenes with electron-donor and/or electron-withdrawing substituents are precipitated from the vapor phase and solution as ultrathin films or nanoparticles with diameter 20–200 nm. The fluorescence quantum yield of the starting oligomers and their alkyl or oxyalkyl derivatives have high quantum yields in solution ($\phi \approx 0.5$), which decreases sharply in films and nanoparticles due to the formation of H-aggregates. However, the emission quantum yield may be raised to ~ 0.7 by the introduction of fluorescent acceptors. Furthermore, the quantum yield can also be increased to ~ 0.6 by increasing the viscosity of the medium, which restricts torsional rotation of the molecular fragments and blocks the transition of the molecules to the twisted intramolecular charge transfer (TICT) state, or upon transition of **77** and **78** to the solid state due to the formation of J-aggregates with a high emission rate constant k_r , which is characteristic both for **77** possessing extremely weak fluorescence in liquid solutions ($\phi \approx 2 \cdot 10^{-3}$) and high quantum yield in the aggregate state or films ($\phi \approx 0.6$) and for **78**. Luminescence quenching in these compounds is due to steric factors caused by a strong deviation from planarity, which increases the rotation-induced nonradiative deactivation. Figure 15 shows that the luminescence bands of **77** and **78** are strongly shifted relative to their bands in the absorption spectra, which indicates a less twisted conformation in the S_1 state [34, 103].



Luminescence of Pairs of Organic Ions and Transition Metal Complexes

An example of AIE caused by the aggregation of pairs of organic ions was given by Lamère et al. [104]. The anionic form of 4-hydroxy-7-nitrobenzoxadiazole (**79**), NBDO⁻, which readily forms a salt with the organic cation tetrabutylammonium bromide (TBAB), served as the fluorescing fragment. The absorption spectrum of undissociated **79** has medium-intensity bands with maxima at 382 and 394 nm, whose position depends on the nature of the solvent. In chloroform, this compound emits very weakly ($\lambda = 2 \cdot 10^{-3}$) in a band with maximum at 554 nm.

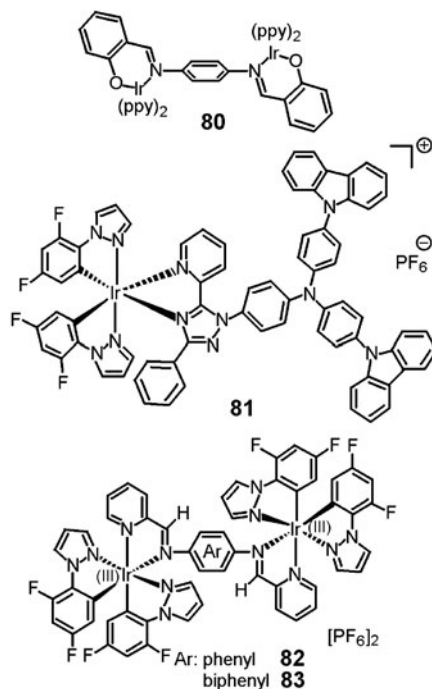
The UV absorption spectra of $\text{TBAB}^+\text{NBDO}^-$ in various solvents are very similar to the spectrum of the NBDO^- ion arising due to dissociation of **79** in water at pH 5.0. The visible absorption spectra show charge transfer bands with maxima at 461 and 468 nm, whose intensity is three times greater than for undissociated **79**. The emission spectrum is independent of the excitation wavelength, which supports the hypothesis of a single emission site. The emission spectrum has bands with maxima at 538 and 586 nm. The quantum yield in all organic solvents is about 10^{-2} but about 10^{-3} in water. The low emission quantum yield of the NBDO^- anion in water may be attributed to the quenching of the excited state of NBDO^- by water molecules. Increased luminescence was observed in the presence of the salt $\text{TBAB}^+\text{NBDO}^-$ formed upon mixing solutions of **79** and TBAB. This increase is related to the formation of fluorescent microcrystals with length up to 60 μm .



Crystals of **79** have a weak luminescence band with maximum at 520 nm and quantum yield $6 \cdot 10^{-3}$, while the emission intensity of the $\text{TBAB}^+\text{NBDO}^-$ microcrystals is much higher. The emission has a band with maximum at 543 nm independently of the excitation wavelength with quantum yield $4.7 \cdot 10^{-2}$. Since the nature of the organic cation may be readily changed, such systems hold interest for the development of new organic luminophores as micro- and nanoparticles, which should emit fluorescence in the solid state and, possibly, in aqueous media.

Little attention has been paid in the literature to the AIE of organometallic and coordination compounds. Phosphorescence is the predominant emission process for most transition metal complexes [105]. Induced aggregation phosphorescent emission has been found for a series of such complexes, for example, with Re(I), Ir(III), Pt(II), Au(I), Zn(II), and Cu(I). As in the case of organic compounds, the emission quantum yield of metal complexes is higher in poor solvents, in which highly-phosphorescent nanoaggregates are formed, which may serve as active components of bio- and chemosensors and optoelectronic devices [106].

Only a few iridium complexes with aggregation-induced phosphorescent emission (AIP) have been studied extensively [107]. Jiang et al. [108] studied the properties of an electroneutral binuclear iridium(III) complex **80**, which displays AIP. Shan et al. [109] have reported an ionic mononuclear iridium(III) complex **81**, which also displays AIP.



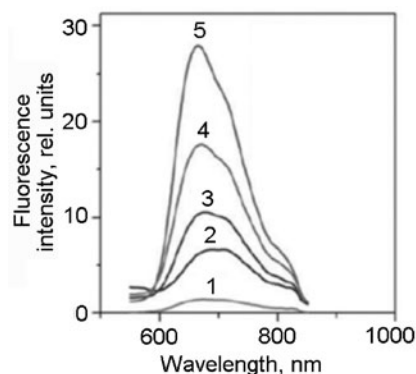
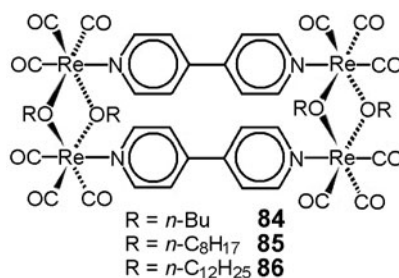


Fig. 16. Fluorescence spectra of **82** in aqueous acetonitrile with water content 0-50 (1), 60 (2), 70 (3), 80 (4), and 90 vol.% (5) at room temperature. Reprinted with permission [110]. Copyright © 2014, The Royal Society of Chemistry.

Binuclear complexes of iridium with diimine ligands (**82**, **83**), which can bind two metal sites, also hold potential for AIP [110]. The electronic spectra of **82** and **83** have predominant absorption bands at 200-300 nm due to spin-resolved $\pi-\pi^*$ transitions of the ligands. The weak absorption in the visible region at 350 nm is related to both metal-ligand and ligand-ligand charge transfer, which is characteristic for iridium(III) complexes. Complexes **82** and **83** hardly emit upon photoexcitation in acetonitrile solution but display intense emission in the film at room temperature with $\lambda_{em} = 644$ and 692 nm, respectively. Thus, **83** is a long-wavelength emitting ionic complex of iridium(III). Complexes **82** (Fig. 16) and **83** in pure acetonitrile display weak emission but when the water content in the mixed solvent is greater than 60 vol.%, the emission intensity is significantly enhanced. The quantum yields of **82** and **83** in a thin film are 0.37 and 0.26, respectively.

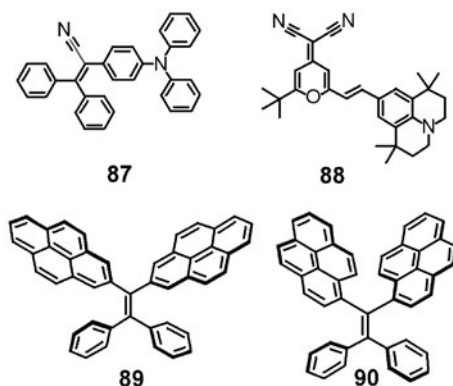
An AIE effect was also observed for rhenium-containing dyes (**84-86**) [111]. True solutions of these compounds do not emit but in media with only moderate solvation, they form luminescent supramolecular aggregates. Thus, the photoluminescence quantum yield of **86** in acetonitrile is only $\phi = 0.39 \cdot 10^{-3}$ but in 1 : 9 acetonitrile-water, this yield is seventeen-fold greater ($\phi = 6.54 \cdot 10^{-3}$) and the emission band maximum undergoes a hypsochromic shift from 666 to 602 nm.



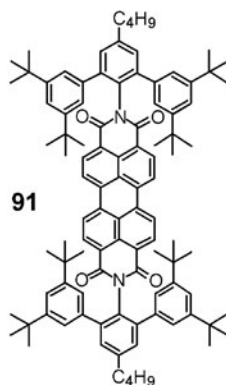
APPLICATIONS OF AGGREGATION-INDUCED EMISSION

Luminescent Solar Concentrators. First-generation dyes including coumarins, perylenes, and rhodamines used in luminescent solar concentrators (LSC) have a number of disadvantages, in particular, concentrational luminescence quenching and small Stokes shifts, which lowers the efficiency of derived LSC [112]. Fluorophores displaying aggregation-induced emission are more promising materials for LSC [113-115]. Such compounds are less susceptible to fluorescence quenching at

high concentrations, which facilitates efficient energy transfer in PMMA films [116]. These processes are seen, for example, using 2-(4-(diphenylamino)phenyl)-3,3-diphenylacrylonitrile (**87**), which displays AIE at high concentrations, as the energy donor and the highly-efficient luminophore of the dye 4-(dicyanomethylene)-2-*tert*-butyl-6-(1,1,7,7-tetramethyljulolidin-9-enyl)-4H-pyran (**88**) at low concentration as the acceptor.



LSC prepared using diphenylethenes of gem-pyrene (**89**, **90**) demonstrate good efficiency and a high quantum yield in the amorphous and crystalline states: 0.14 and 0.39 for **89** and 0.39 and 0.55 for **90**, respectively [113]. LSC using a mixture of an isolated light absorber N,N-(2,6-*bis*(3,5-di-*tert*-butylphenyl)-4-butylphenyl)-perylene diimide **91**, which displays AIE, and perylene red (LR305) increase the efficiency of solar light conversion from 0.68 for individual perylene red to 0.72 for the mixture [117-119].



Optoelectronic Applications. AIE luminophores have now been synthesized with spectral emission encompassing the entire visible and even near-IR range with luminescence quantum yields in the solid state up to unity [120-122]. Such compounds have been used to create organic light diodes with both monochromatic red, green, and blue emission as well as white light emission [123, 124]. AIE compounds with delayed fluorescence consisting of carbazolyl- and phenothiazinyl-substituted benzophenones are used for the manufacture of single-component AIE luminogens emitting white light. Such compounds demonstrate great potential for use in the development of simple and efficient devices for the emission of white light [125].

Another area of study, in which the AIE luminogens may be used, is in liquid crystal displays [126]. Liquid crystals are non-emitting compounds and require backlighting for screen displays, complex design, and high energy consumption. Virtually any such display has an active matrix of transistors used to form the image, a layer of liquid crystals with light filters for selective light transmission, and a backlighting system, as a rule, consisting of light diodes. The latter is necessary for the display of color images. Liquid crystals derived from AIE systems give bright emission in the solid state, especially, in the highly-ordered crystalline state. Such substances provide a unique possibility of preparing light-emitting liquid crystal displays of simplified construction requiring lower energy consumption. Circularly polarized luminescence (CPL) provides for the

possibility of the transmission of stereochemical, conformational, and three-dimension-structural information, which is extremely necessary for 3D displays. In contrast to traditional materials of this type with a fluorescence quenching effect, AIE-active materials with CPL demonstrate intense fluorescence, strong circular dichroism signals, and high CPL dissymmetry coefficients in films, which has great importance for further improvements of 3D displays [127].

Environmental Monitoring. The detection of ions of various compounds is one of the major problems in monitoring the environment since they play an important role in metabolism and biological systems. Coumarin and α -cyanostilbene were used to synthesize a selective and sensitive probe for the detection of Hg^{2+} ions based on the AIE effect. This probe has weak fluorescence in solutions and enhanced emission in the solid state due to the formation of excimers and a π - π stacking interaction of the coumarin groups [128].

Huerta-Aguilar et al. [129] described the fluorescence of a Schiff base, which can serve as a fluorescent probe, namely, *N,N'*-propylene-*bis*(salicylimine) (salpn), for the detection of Al^{3+} ions with detection threshold $1.24 \cdot 10^{-3}$ mmol/L. Spherical fluorescent organic nanoparticles (FON) with diameter 100 nm acting as chemosensors have been obtained using salpn. The observed luminescence intensity enhancement of salpn FON in the presence of Al^{3+} ions may be ascribed to enhanced fluorescence due to chelation of the receptor bound to Al^{3+} ions, which imparts rigidity to the system and the formation of J-aggregates.

Tetraphenylimidazole derivatives, which may form FON with AIE characteristics, were used to synthesize 2-(4-(1,4,5-triphenyl-1H-imidazol-2-yl)benzylidene)malononitrile (TIBM) for the selective detection of sulfites in the air, food products, and biological systems. When used with cetyltrimethylammonium bromide as a surfactant, this compound can assemble into well-organized nanoparticles, which are the basis of a nanosensor with a rapid response (15 s), high selectivity, and extremely low sulfite detection threshold (7.4 nM) in various media [130].

2-(2'-Hydroxyphenyl)benzimidazole (HPBI) is an active AIE fluorophore and demonstrated four-fold greater emission upon aggregation in comparison with the aqueous solution. The penetration of the aggregated structures into living cells makes HPBI an efficient system for studying cell deformation since the monomers do not give any visible fluorescence within cells [131].

2-(Trityliminomethyl)-quinolin-8-ol (HL), which displays an AIE effect, is a chemosensor for the detection of Zn^{2+} ions in a ZnL_2 complex with high selectivity and sensitivity in aqueous media. ZnL_2 also fluoresces in the solid state. The emission intensity of ZnL_2 in aqueous THF increases by a factor of 178 with an increase in the water fraction from 60% to 75%, apparently due to the formation of J-aggregates; the quantum yield reaches 0.33 (in pure THF, $\phi = 0.029$). Furthermore, HL may efficiently detect intracellular Zn(II) ions due to the ESIPT process related to the AIE property of ZnL_2 in the mixed solvent [132].

AIE probes have been developed for the detection of CN^- ions [133]. AIE systems have also shown promise for the detection of other ecologically-important compounds such as carbon dioxide [134], primary amines [135], and hydrogen sulfide [136].

The quenching of the fluorescence of AIE luminogens by various electron receptors has opened additional possibilities for monitoring 2,4,6-trinitrotoluene [137] and even bacteria and toxins, which was stressed in a Faraday Discussions article related to their practical application [138].

Biological and Biomedical Applications. The use of fluorescent probes based on traditional fluorogens is complicated by fluorescence quenching effects, leading to their low selectivity and sensitivity. Clarification of the AIE effect has motivated the development of AIE photoprobes with high signal-to-noise ratio for monitoring biological processes [139, 140]. The first generation of AIE probes for biological detection was based on changes in the fluorescence of water-soluble AIE luminogens due to association-dissociation processes with the analytes used for studying the activity of enzymes and screening inhibitors. The invention of special AIE bioconverters such as peptide AEI conjugates has permitted continuous monitoring of cell apoptosis in real time and the development of biomarkers for cancer cells [141, 142]. This principle also led to the rapid development of various probes for the detection and tracing of various biomolecules and small molecules *in vitro* and *in vivo* [143-145]. Using the unique structure of AIE photosensitizers, the AIE photoprobe can be immediately transformed into a therapeutic probe to perform simultaneous probing, visualization, and therapy [146, 147]. In contrast to traditional photosensitizers characterized by fluorescence quenching and inefficient generation of active oxygen forms in the aggregate

state, AIE photosensitizers as nanoaggregates demonstrate stronger fluorescence, which permits the accumulation of higher active oxygen concentrations.

Light probes with activated photoactivity have been developed for the controlled ablation of cancer cells [146, 148, 149]. Similar probes have been found effective for the detection, visualization, and ablation of bacteria [150, 151].

AIE dots have been developed using the pronounced emission of AIE luminogens in the aggregated state. Such AIE dots are very small organic nanoparticles displaying strong brightness, high resistance to photodecoloration, and excellent biocompatibility. These properties are used in the target cell and for subcellular visualization as well as for monitoring cancer cells *in vitro* and *in vivo* [152-155]. The recent development of AIE dots with emission in the near-IR region has opened new and expanded possibilities for visualization, operational surgery, and therapy [156].

CONCLUSION

The results reviewed in this article on aggregation-induced emission phenomena demonstrate the undoubted importance of this effect for the development of the photonics of organic molecules and nanostructures, a deeper understanding of the mechanisms leading to radiative photoexcitation energy consumption in the aggregate state, and elucidation of the nature of nonradiative processes leading to luminescence quenching both in solutions and various aggregates of organic compounds. Although these fundamental photophysical processes have been examined before the formulation of the AIE concept and mechanisms have been proposed to explain aggregative fluorescence quenching, it would appear that new models should be developed to interpret AIE processes. In this review, attention was focused on three fundamental AIE mechanisms but they should be considered as elements of a single working model for AIE, namely, hindrance to intramolecular motions. A mechanistic picture for the AIE process can be represented as hindrance of dynamic intramolecular motions, namely, low-frequency vibrational and rotation modes of energy reorganization involved in the nonradiative dissipation of the excited state energy of an AIE luminogen. The efficiency of radiative channels for the dissipation of electronic excitation energy and emission intensity is enhanced due to hindrance of such motion.

Whether a luminogen will possess an AIE effect depends largely on the conformational flexibility and amplitude of the motions of its molecules. The quenching of the emission of solutions is a key factor in the AIE of a structurally-flexible luminogen, which is the result of the consumption of energy required to perform intramolecular motions. AIE luminogens, as a rule, are nonplanar molecules not displaying luminescent properties as isolated molecules. Thus, it was considered until recently that a poor light emitter in the dissolved state cannot emit efficiently in the solid state. However, AIE shows that this concept is not always correct. A weak emitter in a dilute solution can be an efficient emitter in the solid state. This finding expands the scope of the search for efficient light-emitting solid materials, which may be employed in nanophotonic devices for various purposes.

There has recently been exponential growth in theoretical and applied studies of AIE, which opens broad prospects for its practical use. From the viewpoint of designing new materials possessing AIE, there has been a tendency move away from the synthesis of simple AIE molecules to more functionalized structures, combining organic AIE luminogens with other organic and inorganic components or building blocks on the molecular and mesoscopic levels for the development of multifaceted luminogens such as metal organic frameworks derived from AIE luminogens and AIE metal complexes. The rational construction, especially of modular hybrid structures, may lead to advanced functional materials and systems with still greater potential for use in energy devices, environmental monitoring, biomedical investigations including the visualization *in vitro* and *in vivo* of biological structures such as organelles, cells, and tissues and the study of cell processes such as apoptosis and metastases. In addition, it is important to elucidate the fundamental mechanisms of the functioning of such new materials and systems, the interrelationship between their structure and properties, and the factors affecting molecular packing and polymorphism of the resultant nanostructures, which determine their AIE properties.

Thus, AIE luminogens have proven to be simple but very useful components of a series of nanophotonic systems and instruments in the monitoring of many important physical and biological processes. In the next few years, we can expect further developments in the photonics of organic compounds and nanostructures and that the results of these investigations will find use in the solution of complex problems that have proven resistant to solution by traditional strategies.

REFERENCES

1. S. V. Gaponenko, *Optical Properties of Semiconductor Nanocrystals*, University Press, Cambridge (1998).
2. A. Rogach (ed.), *Semiconductor Nanocrystal Quantum Dots. Synthesis, Assembly, Spectroscopy, and Applications*, Springer, New York (2008).
3. J. Lakowicz, C. Geddes, I. Gryczynski, et al., *J. Fluoresc.*, **14**, No. 4, 425-441 (2004).
4. C. J. Murphy, T. K. Sau, A. Gole, et al., *J. Phys. Chem. B*, **109**, No. 29, 13857-13870 (2005).
5. M. E. Stewart, C. Anderton, B. Thompson Lucas, et al., *Chem. Rev.*, **108**, No. 2, 494-521 (2008).
6. E. Botzung-Appert, V. Monnier, T. Ha Duong, et al., *Chem. Mater.*, **16**, No. 9, 1609-1611 (2004).
7. H. Y. Kim, T. G. Bjorklund, S.-H. Lim, and C. J. Bardeen, *Langmuir*, **19**, 3941-3946 (2003).
8. J. Wenus, S. Ceccarelli, D. G. Lidzey, et al., *Org. Electron.*, **8**, Nos. 2/3, 120-126 (2007).
9. J. Luo, Z. Xie, B. Z. Tang, et al., *Chem. Commun.*, No. 18, 1740-1741 (2001).
10. J. Chen, Ch. C. W. Law, B. Z. Tang, et al., *Chem. Mater.*, **15**, No. 7, 1535-1546 (2003).
11. J. Chen, Z. Xie, B. Z. Tang, et al., *Macromolecules*, **36**, No. 4, 1108-1117 (2003).
12. C. L. Vonnegut, B. W. Tresca, D. W. Johnson, et al., *Chem. Asian J.*, **10**, No. 3, 522-535 (2015).
13. R. Deans, J. Kim, M. R. Machacek, et al., *J. Am. Chem. Soc.*, **122**, No. 35, 8565-8566 (2000).
14. C. Belton, D. F. O'Brien, W. J. Blau, et al., *Appl. Phys.*, **78**, No. 8, 1059-1061 (2001).
15. C. H. Zhao, H. Sakuda, W. Wakamiya, and S. Yamaguchi, *Chem. Eur. J.*, **15**, No. 40, 10603-10612 (2009).
16. H.-B. Fu and J.-N. Yao, *J. Am. Chem. Soc.*, **123**, No. 7, 1434-1439 (2001).
17. B.-K. An, S.-K. Kwon, S.-D. Jung, et al., *J. Am. Chem. Soc.*, **124**, No. 48, 14410-14415 (2002).
18. Y. Liu, Y. Youhong Tang, N. N. Barashkov, et al., *J. Am. Chem. Soc.*, **132**, No. 40, 13951-13953 (2010).
19. N. N. Barashkov, Yu. E. Sakhno, V. M. Granchak, et al., *International Conference on Modern Physical Chemistry for Advanced Materials*, Kharkov, Ukraine, June 26-30, 2007, <http://www.certh.gr/dat/F5BD8DC3/file.pdf>.
20. Yuning Hong, W. Y. Lam Jacky, and Ben Zhong Tang, *Chem. Soc. Rev.*, **40**, No. 11, 5361-5388 (2011).
21. A. A. Ishchenko and S. A. Shapovalov, *J. Appl. Spectrosc.*, **71**, No. 5, 605-629 (2004).
22. A. D. Nekrasov, B. I. Shapiro, A. I. Tolmachev, et al., *Khim. Vysok. Énerg.*, **45**, No. 6, 563-569 (2011).
23. E. G. McRae and M. Kasha, *J. Chem. Phys.*, **28**, No. 4, 721-722 (1958).
24. N. Kh. Ibrayev, S. A. Yeroshina, A. A. Ishchenko, and I. L. Mushkalo, *Mol. Cryst. Liq. Cryst.*, **427**, No. 1, 139-147 (2005).
25. N. Kh. Ibraev, A. A. Ishchenko, R. Kh. Karamysheva, and I. L. Mushkalo, *J. Lumin.*, **90**, Nos. 3/4, 81-88 (2000).
26. H. Kasai, Y. Yoshikawa, T. Seko, et al., *Mol. Cryst. Liq. Cryst.*, **294**, No. 1, 173-176 (1997).
27. H. Kasai, H. Kamatani, S. Okada, et al., *Jpn. J. Appl. Phys.*, **35**, Pt 2, No. 2B, L221-L223 (1996).
28. H. Kasai, H. Kamatani, Y. Yoshikawa, et al., *Chem. Lett.*, **26**, No. 11, 1181-1182 (1997).
29. Y. Komai, H. Kasai, H. Hirakoso, et al., *Mol. Cryst. Liq. Cryst.*, **322**, No. 1, 167-172 (1998).
30. Y. Xu, P. Xue, D. Xu, et al., *Org. Biomol. Chem.*, **8**, No. 19, 4289-4296 (2010).
31. M. Martínez-Abadía, B. Robles-Hernández, M. R. de la Fuente, et al., *Adv. Mater.*, **28**, No. 31, 6586-6591 (2016).
32. Xing-Liang Peng, Sergi Ruiz-Barragan, Ze-Sheng Li, et al., *J. Mater. Chem. C*, **4**, No. 14, 2802-2810 (2016).
33. M. Martínez-Abadía, S. Varghese, R. Giménez, and M. B. Ros, *J. Mater. Chem. C*, **4**, No. 14, 2886-2893 (2016).
34. D. Oelkrug, A. Tompert, J. Gierschner, et al., *J. Phys. Chem. B*, **102**, No. 11, 1902-1907 (1998).
35. M. M. Souza, G. Rumbles, I. R. Gould, et al., *Synth. Met.*, **111/112**, 539-543 (2000).
36. C. Zhao, Z. Wang, Y. Yang, et al., *Cryst. Growth Des.*, **12**, No. 3, 1227-1231 (2012).
37. Fuke Wang, Ming-Yong Han, Khine Yi Mya, et al., *J. Am. Chem. Soc.*, **127**, No. 29, 10350-10355 (2005).
38. F. Ito, T. Sagawa, and H. Koshiyama, *Res. Chem. Intermed.*, **41**, No. 9, 6897-6906 (2015).
39. N. N. Barashkov, T. V. Sakhno, R. N. Nurmukhametov, and O. A. Khakhel', *Usp. Khim.*, **66**, No. 6, 579-593 (1993).
40. F. Ito, T. Kakiuchi, T. Sakano, and T. Nagamura, *Phys. Chem. Chem. Phys.*, **12**, No. 36, 10923-10927 (2010), doi: 10.1039/c003023f.
41. R. L. Penn and J. F. Banfield, *Science*, **281**, No. 5379, 969-971 (1998).
42. Y. Qian, S. Li, G. Zhang, et al., *J. Phys. Chem. B*, **111**, No. 21, 5861-5868 (2007).
43. Li Qiang Yan, Zhi Neng Kong, Yong Xia, and Zheng Jian Qi, *New J. Chem.*, **40**, No. 8, 7061-7067 (2016).

44. S. Li, L. He, F. Xiong, et al., *J. Phys. Chem. B*, **108**, No. 30, 10887-10892 (2004).
45. C. Feng, J. Li, X. Han, et al., *Faraday Discuss.*, **196**, 163-176 (2017).
46. R. Hu, E. Lager, and A. Aguilar-Aguilar, *J. Phys. Chem. C*, **113**, No. 36, 15845-15853 (2009).
47. A. Aguilar-Granda, S. Pérez-Estrada, A. E. Roa, et al., *Cryst. Growth Des.*, **16**, No. 6, 3435-3442 (2016), doi: 10.1021/acs.cgd.6b00395.
48. Kai Li, Yang Zhang, Bing Qiao, et al., *RSC Adv.*, **7**, No. 48, 30229-30241 (2017).
49. S. K. Behera, A. Murkherjee, G. Sadhuragiri, et al., *Faraday Disc.*, **196**, 71-90 (2017).
50. I. Manikandan, C. H. Chang, and C. L. Chen, *Spectrochim. Acta A*, **182**, 58-66 (2017).
51. M. Han, S. J. Cho, Y. Norikane, et al., *Chemistry*, **22**, No. 12, 3971-3975 (2016).
52. J. Mei, N. L. Leung, R. T. Kwok, et al., *Chem. Rev.*, **115**, No. 21, 11718-11940 (2015).
53. B. Liu and R. Zhang, *Faraday Discuss.*, **196**, 461-472 (2017).
54. Y. Hong, J. W. Y. Lam, and B. Z. Tang, *Chem. Commun.*, No. 29, 4332-4353 (2009).
55. C. J. Bhongale, C.-W. Chang, E. W.-G. Diao, et al., *Chem. Phys. Lett.*, **419**, Nos. 4-6, 444-449 (2006).
56. T. V. Sakhno, I. V. Korotkova, and O. A. Khakhel', *Teor. Éksp. Khim.*, **32**, No. 4, 247-250 (1996). [*Theor. Exp. Chem.*, **32**, No. 4, 217-220 (1996) (English translation).]
57. T. V. Sakhno, I. V. Korotkova, and O. A. Khakhel', *Funct. Mater.*, **3**, No. 4, 502-505 (1996).
58. T. V. Sakhno, I. V. Korotkova, and N. N. Barashkov, *Zh. Fiz. Khim.*, **71**, No. 5, 861-863 (1997).
59. H. Nie, K. Hu, Y. Cai, et al., *Mater. Chem. Front.*, **1**, No. 5, 1125-1129 (2017).
60. Fan Bu, Erjing Wang, Qian Peng, et al., *Chem. Eur. J.*, **21**, No. 1, 1-11 (2015).
61. J. Gierschner, L. Luer, B. Milian-Medina, et al., *J. Phys. Chem. Lett.*, **4**, No. 16, 2686-2697 (2013).
62. H.-J. Egelhaaf, M. Brun, S. Reich, and D. Oelkrug, *J. Mol. Struct.*, **267**, No. 4, 297-302 (1992).
63. Y. Zhang, L. Kong, J. Shi, et al., *Chin. J. Chem.*, **33**, No. 7, 701-704 (2015).
64. Y. Zhang, H. Mao, L. Kong, et al., *Dyes Pigments*, **133**, 354-362 (2016).
65. A. G. Mirochnik, E. V. Fedorenko, D. Kh. Gizzatulina, and V. E. Karasev, *Zh. Fiz. Khim.*, **81**, No. 11, 2096-2099 (2007).
66. S. A. Tikhonov, V. I. Vovna, I. S. Osmushko, et al., *Spectrochim. Acta A*, **189**, 563-570 (2018).
67. X. Xu, S. Chen, L. Li, et al., *J. Mater. Chem.*, **18**, No. 22, 2555-2561 (2008).
68. S. K. Rajagopal, A. M. Philip, K. Nagarajan, and M. Hariharan, *Chem. Commun.*, **50**, No. 63, 8644-8647 (2014).
69. S. K. Rajagopan, V. S. Reddy, and M. Hariharan, *Cryst. Eng. Commun.*, **18**, No. 27, 5089-5094 (2016).
70. L. G. Samsonova, N. I. Selivanov, and T. N. Kopylova, *Opt. Spektroskop.*, **116**, No. 1, 79-84 (2014).
71. M. L. Ferrer and F. del Monte, *J. Phys. Chem. B*, **109**, No. 1, 80-86 (2005).
72. G. Quian, B. Dai, M. Luo, et al., *Chem. Mater.*, **20**, No. 19, 6208-6216 (2008).
73. W. Tang, Y. Xiang, and A. Tong, *J. Org. Chem.*, **74**, No. 5, 2163-2166 (2009).
74. Xia Cao, Xi Zeng, Lan Mu, et al., *Sensors Actuators B*, **177**, 493-499 (2013).
75. H. Xiao, K. Chen, D. Cui, et al., *New J. Chem.*, **38**, No. 6, 2386-2393 (2014).
76. C. Niu, L. Zhao, T. Fang, et al., *Langmuir*, **30**, No. 9, 2351-2359 (2014).
77. J. Li, W. Yang, W. Zhou, et al., *RSC Adv.*, **6**, No. 42, 35833-35841 (2016).
78. J. Luo, K. Song, F. L. Gu, et al., *Chem. Sci.*, **2**, No. 10, 2029-2034 (2011).
79. N. L. C. Leung, N. Xie, W. Yuan, et al., *Chem. Eur. J.*, **20**, No. 47, 15349-15353 (2014).
80. T. Nishiuchi, K. Tanaka, and Y. Yoshiyuki Kuwatani, et al., *Chem. Eur. J.*, **19**, No. 13, 4110-4116 (2013).
81. C. Yuan, S. Saito, C. Camacho, et al., *Chem. Eur. J.*, **20**, No. 8, 2193-2200 (2014).
82. C.-X. Yuan, X.-T. Tao, Y. Ren, et al., *J. Phys. Chem. C*, **111**, No. 34, 12811-12816 (2007).
83. J. Liu, Q. Meng, X. Zhang, et al., *Chem. Commun.*, **49**, No. 12, 1199-1201 (2013).
84. K. S. N. Kamaldeep, S. Kaur, V. Bhalla, et al., *J. Mater. Chem. A*, **2**, No. 22, 8369-8375 (2014).
85. S. Kaur, A. Gupta, V. Bhalla, et al., *J. Mater. Chem. C*, **2**, No. 35, 7356-7363 (2014).
86. E. Cariati, V. Lanzani, E. Tordin, et al., *Phys. Chem. Chem. Phys.*, **13**, No. 40, 18005-18014 (2011).
87. Bin Wang, Xiaojuan Wang, Wenliang Wang, and Fengyi Liu, *J. Phys. Chem. C*, **120**, No. 38, 21850-21857 (2016).
88. N. J. Hestand and F. C. Spano, *Accounts Chem. Res.*, **50**, No. 2, 341-350 (2017).
89. W. I. Gruzeccki, *J. Biol. Phys.*, **18**, No. 2, 99-109 (1991).

90. W. I. Gruzecki, B. Zelent, and R. M. Leblanc, *Chem. Phys. Lett.*, **171**, Nos. 5/6, 563-568 (1990).
91. N. Ramesh and A. Patnaik, *J. Phys. Chem. C*, **120**, No. 3, 1909-1917 (2016).
92. A. A. Muentner, D. V. Brumbaugh, J. J. Apolito, et al., *J. Phys. Chem.*, **96**, No. 7, 2783-2790 (1992).
93. J. Gierschner and S. Y. Park, *J. Mater. Chem. C*, **1**, No. 37, 5818-5832 (2013).
94. L. M. Nikolenko and A. V. Ivanchikhina, *Khim. Vysok. Énerg.*, **44**, No. 6, 1-9 (2010).
95. B. Bhattacharyya, A. Kundu, A. Das, et al., *RSC Adv.*, **6**, No. 26, 21907-21916 (2016).
96. D. A. Nosova, E. P. Zarochentseva, S. O. Vysotskaya, et al., *Opt. Spektroskop.*, **117**, No. 6, 907-913 (2014).
97. B. I. Shapiro, L. S. Sokolova, V. A. Kuz'min, et al., *Nanotechnol. in Russia*, **7**, Nos. 5/6, 205-212 (2012).
98. B.-K. An, J. Gierschner, and S. Y. Park, *Accounts Chem. Res.*, **45**, No. 4, 544-554 (2012).
99. S. Ozcelik and D. L. Akins, *J. Phys. Chem. B*, **103**, No. 42, 8926-8929 (1999).
100. B. Zhang, W. Diao, C. Bi, et al., *J. Fluoresc.*, **22**, No. 1, 1-7 (2012).
101. T. V. Sakhno, I. V. Korotkova, N. N. Barashkov, and J. P. Ferraris, *SPIE, Partenit, Crimea, Ukraine, 5-10 October, 1997*, 3488, pp. 284-292.
102. D. Oelkrug, A. Tompert, H.-J. Egelhaaf, et al., *Synth. Met.*, **83**, No. 3, 231-237 (1996).
103. F. Lange, D. Hohnholz, M. Leuze, et al., *Synth. Met.*, **101**, No. 1, 652-653 (1999).
104. J. F. Lamère, N. Saffon, I. D. Santos, and S. Fery-Forgues, *Langmuir*, **26**, No. 12, 10210-10217 (2010).
105. L. Ravotto and P. Ceroni, *Coord. Chem. Rev.*, **346**, 62-76 (2017).
106. V. Sathish, A. Ramdass, P. Thanasekaran, and K.-L. Lu, *J. Photochem. Photobiol. C*, **23**, 25-44 (2015).
107. P. Alam, S. Dash, C. Climent, et al., *RSC Adv.*, **7**, No. 10, 5642-5648 (2017).
108. Yang Jiang, Guangfu Li, Weilong Che, et al., *Chem. Commun.*, **53**, No. 21, 3022-3025 (2017).
109. G. G. Shan, H. B. Li, J. S. Qin, et al., *Dalton Trans.*, **41**, No. 32, 9590-9593 (2012).
110. G. F. Li, Y. Wu, G. G. Shan, et al., *Chem. Commun.*, **50**, No. 53, 6977-6980 (2014).
111. P. Thanasekaran, J. Y. Wu, B. Manimaran, et al., *J. Phys. Chem. A*, **111**, No. 43, 10953-10960 (2007).
112. V. M. Granchak, T. V. Sakhno, and S. Ya. Kuchmy, *Teor. Éksp. Khim.*, **50**, No. 1, 1-20 (2014) [*Theor. Exp. Chem.*, **50**, No. 1, 1-20 (2014) (English translation).]
113. J. L. Banal, J. M. White, K. P. Ghiggino, et al., *Sci. Rep.*, **4**, 4635 (2014).
114. Kok-Haw Ong and Bin Liu, *Molecules*, **22**, No. 6, 897 (2017), doi: 10.3390/molecules22060897.
115. Guangxue Feng, T. K. Kwok Ryan, Ben Zhong Tang, and Bin Liu, *Appl. Phys. Rev.*, **4**, 021307 (2017).
116. J. L. Banal, K. P. Ghiggino, and W. W. H. Wong, *Phys. Chem. Chem. Phys.*, **16**, No. 46, 25358-25363 (2014).
117. J. L. Banal, J. M. White, T. W. Lam, et al., *Adv. Energy Mater.*, **5**, 1500818 (2015).
118. J. L. Banal, H. Soleimaninejad, F. M. Jradi, et al., *J. Phys. Chem. C*, **120**, No. 24, 12952-12958 (2016).
119. B. Zhang, J. L. Banal, D. J. Jones, et al., *Mater. Chem. Front.*, **2**, No. 3, 615-619 (2018).
120. Z. J. Zhao, J. W. Y. Lam, and B. Z. Tang, *J. Mater. Chem.*, **22**, No. 45, 23726-23740 (2012).
121. Y. H. Liu, C. Mu, K. Jiang, et al., *Adv. Mater.*, **27**, No. 6, 1015-1020 (2015).
122. Y. Hong, *Methods Appl. Fluoresc.*, **4**, 022003 (2016).
123. W. Qin, Z. Yang, Y. Jiang, et al., *Chem. Mater.*, **27**, No. 11, 3892-3901 (2015).
124. B. Liu, H. Nie, X. Zhou, et al., *Adv. Function. Mater.*, **26**, No. 5, 776-783 (2016).
125. Z. L. Xie, C. J. Chen, S. D. Xu, et al., *Angew. Chem. Int. Ed.*, **54**, No. 24, 7181-7184 (2015).
126. D. Zhao, Fan Fan, Cheng Juan, et al., *Adv. Opt. Mater.*, **3**, No. 2, 199-202 (2015).
127. J. Liu, H. Su, L. Meng, et al., *Chem. Sci.*, **3**, No. 9, 2737-2747 (2012).
128. G. Zhang, X. Zhang, Y. Zhang, et al., *Sensors Actuators B*, **221**, 730-739 (2015).
129. C. A. Huerta-Aguilar, P. Raj, P. Thangarasu, and N. Singh, *RSC Adv.*, **6**, No. 44, 37944-37952 (2016).
130. Tang Guo, Xiaozheng Cao, Peng Ge, et al., *Org. Biomol. Chem.*, **15**, No. 20, 4375-4382 (2017).
131. A. Malakar, M. Kumar, A. Reddy, et al., *Photochem. Photobiol. Sci.*, **15**, No. 7, 937-948 (2016), doi: 10.1039/c6pp00122j.
132. Dan Wang, Shu-Mu Li, Jian-Quan Zheng, et al., *Inorg. Chem.*, **56**, No. 2, 984-990 (2017).
133. Y. R. Li, H. T. Zhou, W. Chen, et al., *Tetrahedron*, **72**, No. 36, 5620-5625 (2016).
134. T. Tian, X. Chen, H. Li, et al., *Analyst*, **138**, No. 4, 991-994 (2013).
135. T. Han, J. W. Lam, N. Zhao, et al., *Chem. Commun.*, **49**, No. 42, 4848-4850 (2013).

136. Y. Cai, L. Li, Z. Wang, et al., *Chem. Commun.*, **50**, No. 64, 8892-8895 (2014).
137. J. H. Wang, H. T. Feng, and Y. S. Zheng, *Chem. Commun.*, **50**, No. 77, 11407-11410 (2014).
138. Ruoyu Zhang, Xiaolei Cai, Guang Feng, and Ben Liu, *Faraday Discuss.*, **196**, 363-375 (2017).
139. M. Wang, G. Zhang, D. Zhang, et al., *J. Mater. Chem.*, **20**, No. 10, 1858-1867 (2010).
140. J. Liang, B. Z. Tang, and B. Liu, *Chem. Soc. Rev.*, **44**, No. 10, 2798-2811 (2015).
141. H. Shi, J. Liu, J. Geng, et al., *J. Am. Chem. Soc.*, **134**, No. 23, 9569-9572 (2012).
142. H. Shi, R. T. K. Kwok, J. Liu, et al., *J. Am. Chem. Soc.*, **134**, No. 43, 17972-17981 (2012).
143. D. Ding, K. Li, B. Liu, and B. Z. Tang, *Accounts Chem. Res.*, **46**, No. 11, 2441-2453 (2013).
144. R. T. Kwok, C. W. Leung, J. W. Lam, et al., *Chem. Soc. Rev.*, **44**, No. 13, 4228-4238 (2015).
145. H. Gao, X. Zhao, and S. Chen, *Molecules*, **23**, No. 2, 419-439 (2018).
146. Y. Y. Yuan, C. J. Zhang, M. Gao, et al., *Angew. Chem. Int. Ed.*, **54**, No. 6, 1780-1786 (2015).
147. Y. Y. Yuan, S. D. Xu, X. M. Cheng, et al., *Angew. Chem. Int. Ed.*, **55**, No. 22, 6457-6461 (2016).
148. Y. Y. Yuan, C. J. Zhang, S. D. Xu, and B. Liu, *Chem. Sci.*, **7**, No. 3, 1862-1866 (2016).
149. F. Hu, Y. Y. Huang, G. X. Zhang, et al., *Anal. Chem.*, **86**, No. 15, 7987-7995 (2014).
150. G. X. Feng, Y. Y. Yuan, H. Fang, et al., *Chem. Commun.*, **51**, No. 62, 12490-12493 (2015).
151. E. G. Zhao, Y. L. Chen, S. J. Chen, et al., *Adv. Mater.*, **27**, No. 33, 4931-4937 (2015).
152. W. Qin, D. Dan, J. Z. Liu, et al., *Adv. Funct. Mater.*, **22**, No. 4, 771-779 (2012).
153. K. Li, W. Qin, D. Ding, et al., *Sci. Rep.*, **3**, 1150-1156 (2013).
154. D. Ding, D. Mao, K. Li, et al., *ACS Nano*, **8**, No. 12, 12620-12631 (2014).
155. L. L. Yan, Y. Zhang, B. Xu, et al., *Nanoscale*, **8**, No. 5, 2471-2487 (2016).
156. J. Liu, C. Chen, S. Ji, et al., *Chem. Sci.*, **8**, No. 4, 2782-2789 (2017).